Exclusive $N^* \rightarrow KY$ Studies with CLAS12

Daniel S. Carman *(contact person, spokesperson)*, Victor Mokeev *(spokesperson)*,
Harut Avakian, Volker Burkert, Eugene Pasyuk
Jefferson Laboratory, Newport News, VA 23606, USA

Robert G. Edwards, Michael R. Pennington, David G. Richards, Adam P. Szczepaniak[†]
Theory Center, Jefferson Laboratory, Newport News, VA 23606, USA
([†] *Joint with Indiana University, Bloomington, IN 47405*)

Hiroyuki Kamano
Research Center for Nuclear Physics, Osaka University, Ibaraki, Osaka 567-0047, Japan

Bill Briscoe, Michael Döring, Diane Schott, Igor Strakovsky, Ron Workman
The George Washington University, Washington, DC 20052, USA

Ralf Gothe *(spokesperson)*
University of South Carolina, Columbia, SC 29208, USA

T.-S. Harry Lee, Craig D. Roberts
Argonne National Laboratory, Argonne, IL 60439, USA

Jan Ryckebusch
Ghent University, B-9000 Ghent, Belgium

Dave Ireland
University of Glasgow, Glasgow G12 8QQ, United Kingdom

Kijun Park
Old Dominion University, Norfolk, VA 23529

Brian Raue
Florida International University, Miami, FL 33199

Evgeny Golovach, Boris Ishkhanov, Evgeny Isupov
Skobeltsyn Nuclear Physics Institute, Moscow State University, 119899, Moscow, Russia

Haiyun Lu
University of Iowa, Iowa City, IA 52242

Ken Hicks
Ohio University, Athens, OH 45701

and the CLAS Collaboration

A New Research Proposal Submitted to Jefferson Lab PAC42

Abstract

We propose to measure KY electroproduction cross sections from an unpolarized proton target with a focus on the $K^+\Lambda$ and $K^+\Sigma^0$ final states to study high-lying nucleon excited states (N^*) with the CLAS12 detector at a beam energy of 11 GeV. Exclusive final states will be measured, including the identification of the scattered electron and the electroproduced K^+. From these data, the electromagnetic transition form factors $\gamma_v NN^*$ for the most prominent N^* and Δ^* states decaying to KY will be extracted in the range of invariant energy $1.6 < W < 3$ GeV in the virtually unexplored domain of momentum transfers Q^2 from 4 to 12 GeV^2. This experiment is an essential component of a comprehensive program of exclusive electroproduction measurements with CLAS12 studying decays of N^* states to a number of different final state channels. Analysis of these data for the strangeness channels will be carried out in concert with the group working to extract the electrocoupling parameters from the non-strange single meson and $N\pi\pi$ final states from CLAS12 data. The close collaboration of experimentalists and theorists is a necessary part of this proposal in order to provide high quality analysis of the collected data to perform state-of-the-art model and QCD-based calculations. The main goal of this proposal is to explore the evolution of the active degrees of freedom in N^* states from the regime of meson-baryon dressing at lower Q^2 to the regime of dressed quark contributions at higher Q^2. In addition, these data will allow us to better understand how the strong interaction creates dressed quark cores in various N^* resonances and to better understand their emergence from QCD, as well as to study evidence for the coupling of produced hybrid baryon states to these KY channels.

Contents

1 Introduction

Detailed spectroscopic studies of the nucleon excitation spectrum and the structure of these excited states have played a central role in the development of our understanding of the dynamics of the strong interaction. The concept of quarks that emerged through such studies led to the development of the constituent quark model [1] (CQM) in the 1980s. As a result of intense experimental and theoretical effort over the past 30 years, it is now apparent that the structure of the nucleon and its spectrum of excited states (N^*) are much more complex than what can be described in terms of models based on constituent quarks alone. The structure of low-lying baryon states, as revealed by electromagnetic probes at low momentum transfer ($Q^2 < 2$ GeV^2), has been shown to be reasonably well described by adding meson-baryon effects (e.g. a meson-baryon cloud) phenomenologically to the basic CQM [2, 3, 4]. However, a fundamental understanding of N^* structure at short distances, which is only accessible using probes with sufficiently high momentum transfer, necessarily demands use of the full complexities of Quantum Chromodynamics (QCD). Studies of the Q^2 evolution of N^* structure offer access to the strong interaction between dressed quarks in the non-perturbative regime, which is responsible for N^* formation. Moreover, the range of photon virtualities accessible with CLAS12 allows us to explore the transition from fully dressed constituent quarks to the almost bare current quarks of QCD.

At the typical energy and distance scales found within the N^* states, the quark-gluon coupling is large. Therefore, we are confronted with the fact that quark-gluon confinement, and hence the dynamics of the N^* spectrum, cannot be understood through application of perturbative QCD techniques. The need to understand QCD in this non-perturbative domain is a fundamental issue in nuclear physics that the study of N^* structure can help to address. Such studies, in fact, represent the necessary first steps toward understanding how QCD generates mass, i.e. how mesons, baryons, and atomic nuclei are formed [4].

The study of electroproduction at high Q^2 provides for a probe of the inner structure of the contributing N^* resonances through the extraction of the amplitudes for the transition between the initial virtual photon-nucleon state and the final N^* state, i.e. the $\gamma_v NN^*$ electrocoupling amplitudes, that describe the physics. Among these amplitudes are $A_{1/2}(Q^2)$ and $A_{3/2}(Q^2)$, which describe the resonance electroexcitation for the two different helicity configurations of an initial transverse photon and the nucleon, as well as $S_{1/2}(Q^2)$, which describes the resonance electroexcitation by longitudinal photons of zero helicity. Detailed comparisons of the theoretical predictions for these amplitudes with their experimental measurements is the basis of progress toward understanding non-perturbative QCD.

The extraction of the $\gamma_v NN^*$ electrocouplings provides information on the dynamical momentum-dependent mass and structure of the dressed quark in the non-perturbative domain where the quark-gluon coupling is large. This is critical in exploring the nature of quark-gluon confinement and dynamical chiral symmetry breaking (DCSB) in baryons. Figure 1 illustrates the two contributions to these electrocouplings. In Fig. 1(b) the virtual photon interacts directly with the constituent quark, an interaction that is sensitive to the quark current and depends on the quark-mass function. However, the full meson electroproduction amplitude (Fig. 1(a)) requires contributions to the $\gamma_v NN^*$ vertex from both non-resonant meson electroproduction and the hadronic scattering amplitudes as shown in Fig. 1(c). These contributions incorporate all possible intermediate meson-baryon states and

all possible meson-baryon scattering processes that eventually result in the N^* formation in the intermediate state of the reaction. These two contributions can be separated from each another using, for example, a coupled-channel reaction model [5].

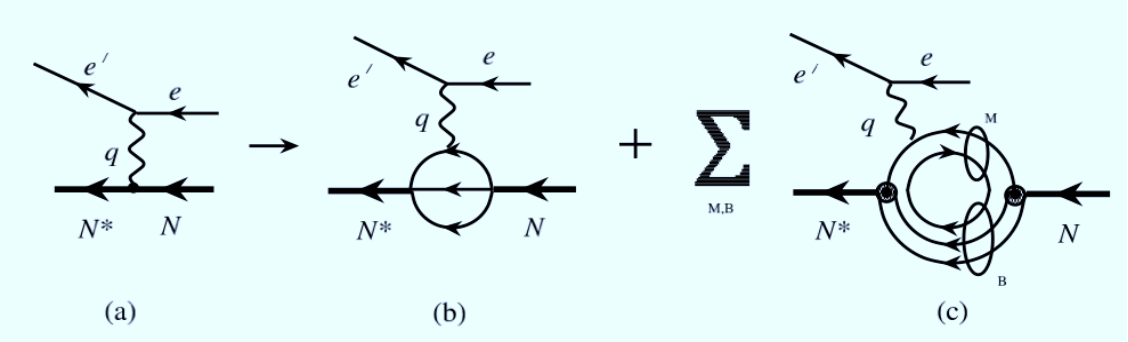

Figure 1: Schematic representation of the $\gamma^* N \to N^*$ electroproduction process. (a). The fully dressed $\gamma_v N N^*$ electrocoupling that determines the N^* contribution to the resonant part of the meson electroproduction amplitude. (b). The contribution of the three-quark core. (c). The contribution from the meson-baryon cloud, where the sum is over all intermediate meson and baryon states. This figure is taken from Ref. [4].

It was found that the structure of N^* states in the range of $Q^2 < 2$ GeV^2 includes important contributions from both diagrams on the right side of Fig. 1. Figure 2 shows several calculations for these contributions to the structure of the low-lying $P_{11}(1440)$ and $D_{13}(1520)$ states. The size of the meson-baryon dressing amplitudes are maximal for $Q^2 < 1$ GeV^2. For $Q^2 > 1$ GeV^2, there is a gradual transition to the domain where the quark degrees of freedom just begin to dominate, as seen by the improved description of the N^* electrocouplings obtained within the framework of these quark models. For $Q^2 > 5$ GeV^2, the quark degrees of freedom are expected to fully dominate the N^* states [6]. Therefore, in the $\gamma_v N N^*$ electrocoupling studies for $Q^2 > 5$ GeV^2, the quark degrees of freedom will be probed more directly with only small contributions from the meson-baryon cloud. This will mark the first opportunity to experimentally study this new and unexplored region in the electroexcitation of nucleon resonances.

A dedicated experiment on studies of N^* structure in exclusive meson electroproduction off the proton with the CLAS12 detector (E12-09-003) [11] has already been approved to provide data to measure exclusive single non-strange meson and double pion electroproduction cross sections over the same Q^2 regime as the data in this proposal. From these cross section measurements, the E12-09-003 Collaboration plans to obtain the electromagnetic transition form factors for all well-established N^* states up to $W \approx 2$ GeV for $5 < Q^2 < 12$ GeV^2. This new proposal represents an extension of that effort to include the strangeness channels coupling via $N^* \to KY$ with $Y = \Lambda, \Sigma$. Note that due to the higher masses of the kaon and hyperons compared with the pionic final states, these reactions kinematically favor a two-body decay mode with masses in the range from 1.6 to 3 GeV. Our plans are to focus our initial efforts in the strangeness sector on measurements of the exclusive $K^+\Lambda$ and $K^+\Sigma^0$ final states as the count rates in the spectrometer are maximal. A second stage of analysis will focus on other final states including $K^0_s\Sigma^+$, K^*Y, and KY^* that will be reconstructed with correspondingly smaller yields.

The invariant mass range of focus for this experiment, $1.6 < W < 3$ GeV, is precisely the

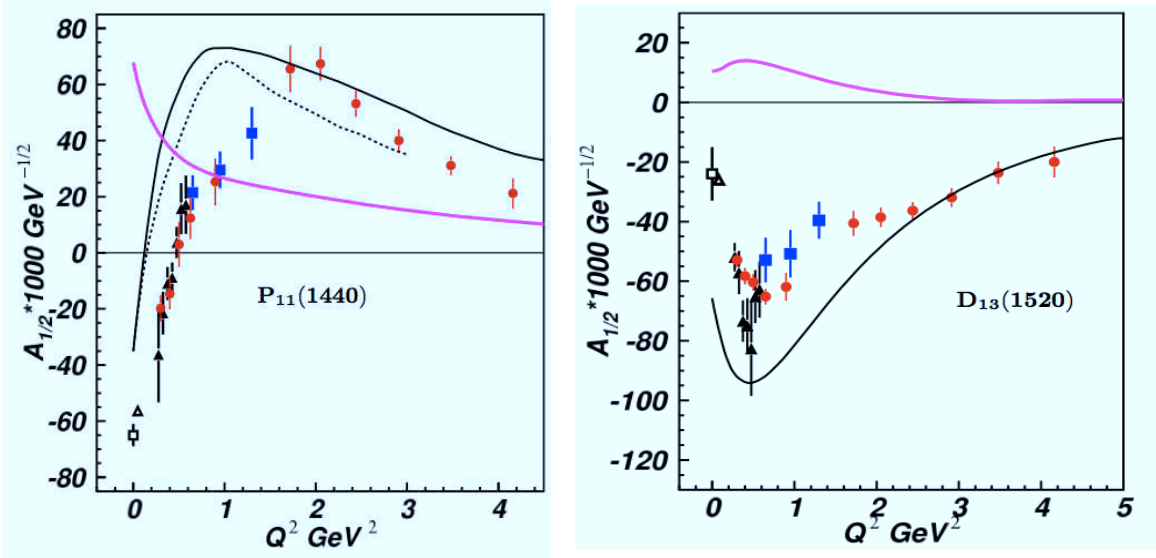

Figure 2: The $A_{1/2}$ electrocoupling amplitudes of the $P_{11}(1440)$ (left) and $D_{13}(1520)$ (right) N^* states from the analyses of the CLAS $N\pi$ data (circles) [7] and $N\pi\pi$ data (triangles, squares) [8]. (Left) Calculations from two relativistic light-front quark models [3, 9] (dashed and black lines). (Right) Calculation from the hypercentral constituent quark model [2] (black line). The magnitude of the meson-baryon cloud contribution as determined by the EBAC coupled-channel analysis [10] is shown by the magenta line in both plots.

mass range where our knowledge of the N^* spectrum and the structure of these excited states is the most limited. While the field has slowly and methodically been making progress toward a better understanding of the low-lying N^* states in the region below 1.6 GeV, the host of the predicted missing N^* and Δ^* states lie in the region from $1.6 < W < 3$ GeV. Figures 3 and 4 show the N^* and Δ^* spectra predicted using the Bonn relativistically covariant quark model [12]. These figures highlight that detailed studies of the mass region provided by the KY final states will be essential to come to a more complete understanding of the structure of the states in the nucleon spectrum. Studies of the structure of the N^* states at higher Q^2 may prove valuable in this regard due to the fact that the ratio of resonant to non-resonant background contributions is expected to improve with increasing photon virtuality. As such we can hope to provide improved information on the poorly known higher-lying N^* states.

Structure studies of the low-lying N^* states, e.g. $P_{33}(1232)$, $P_{11}(1440)$, $D_{13}(1520)$, and $S_{11}(1535)$, have made significant progress in recent years due to the agreement of results from independent analyses of the $N\pi$ and $N\pi\pi$ final states. However, most of the high-lying N^* states with masses above 1.6 GeV decay preferentially through the $N\pi\pi$ channel instead of the $N\pi$ channel. At the current time, the only detailed structure information regarding high-lying N^* states (e.g. $S_{31}(1620)$, $S_{11}(1650)$, $F_{15}(1685)$, $D_{33}(1700)$, and $P_{13}(1720)$) is available from analysis of $N\pi\pi$ data [8]. Data from the KY channels is critical to provide an independent extraction of the electrocoupling amplitudes for the higher-lying N^* states. An important aspect of this proposal is not just the extraction of the $K^+\Lambda$ and $K^+\Sigma^0$ electroproduction cross sections as a function of Q^2, but also a commitment from the E12-09-003 collaborators and theory support group to join with us to further develop their fitting tools to enable extraction of the N^* electrocouplings for the dominant $N^* \rightarrow KY$ hadronic decays from this new proposal.

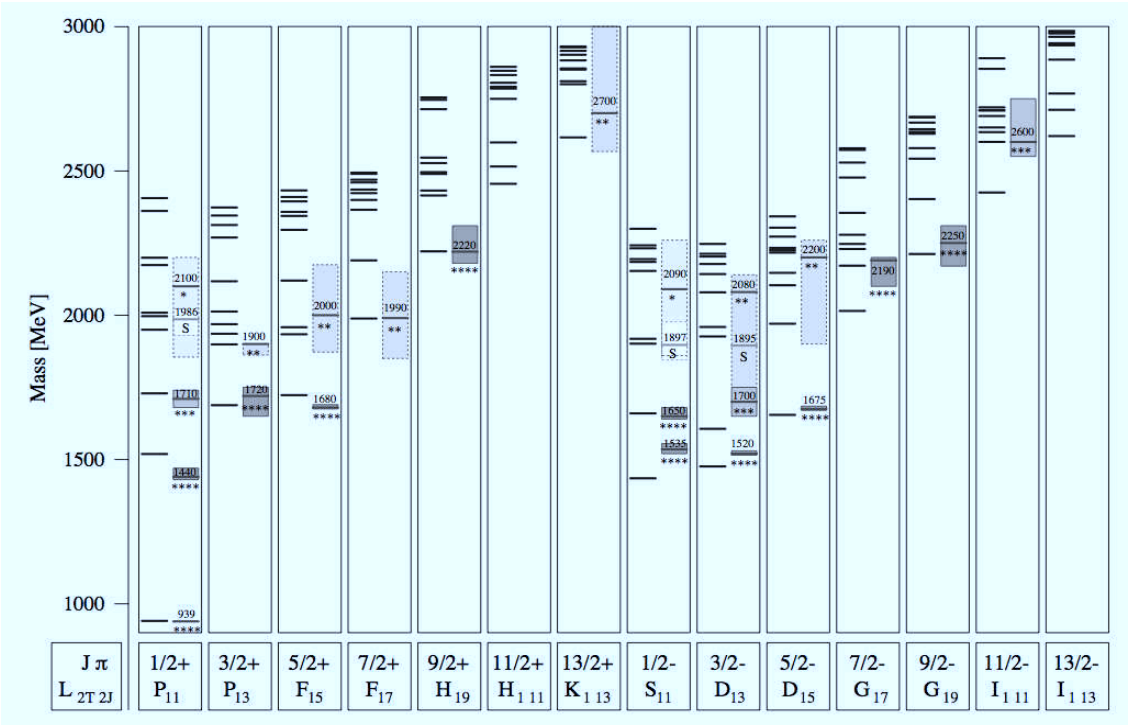

Figure 3: The calculated positive and negative parity N^* spectrum from the Bonn relativistically covariant quark model [12]. The known PDG states [13] are listed in the boxes on the right-hand side of each column.

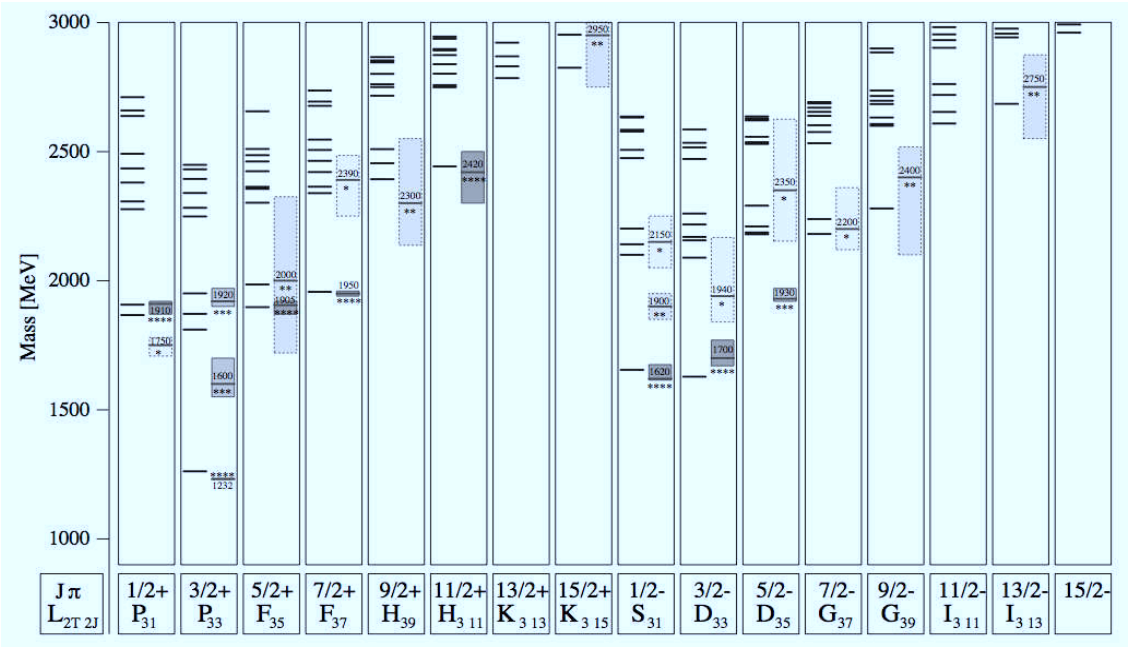

Figure 4: The calculated positive and negative parity Δ^* spectrum from the Bonn relativistically covariant quark model [12]. The known PDG states [13] are listed in the boxes on the right-hand side of each column.

Reliable information on KY hadronic decays from N^*s is not yet available. But the N^* electrocoupling amplitudes can be obtained from fits to the extensive existing CLAS KY electroproduction data over the range $0.5 < Q^2 < 4$ GeV^2 (see Section 3.2), which should be carried out independently in different bins of Q^2. By utilizing the Q^2-independent behavior of resonance hadronic decays, KY electrocouplings will become available from these studies. The development of reaction models for the extraction of the $\gamma_v NN^*$ electrocouplings from the KY electroproduction channels is urgently needed. The work to extract the amplitudes for the prominent N^* and Δ^* states that couple to the strangeness channels $K^+\Lambda$ and $K^+\Sigma^0$ is now getting underway for the CLAS data acquired for $Q^2 < 4$ GeV^2 (see Section 3.5).

Under the aegis of the E12-09-003 proposal, a strong collaboration between experimentalists and theorists has been brought together to achieve the challenging objectives in pursuing N^* studies at high Q^2 [4, 11]. This new proposal to study the $N^* \to KY$ exclusive channels has been developed as an important extension of the CLAS12 N^* program. The main goals of this effort are two-fold:

(i). To develop reaction models for the extraction of the $\gamma_v NN^*$ electrocouplings that incorporate the transition from meson-baryon to quark degrees of freedom into the reaction mechanisms using the data on single-meson (including $n\pi^+$, $p\pi^0$, $p\eta$, $K^+\Lambda$, and $K^+\Sigma^0$) and double charged pion electroproduction ($p\pi^+\pi^-$) off protons for Q^2 up to 12 GeV^2.

(ii). To develop approaches for the theoretical interpretation of the $\gamma_v NN^*$ electrocouplings that are capable of exploring how N^* states are generated non-perturbatively by the strong interaction in processes that emerge from QCD.

Current theoretical approaches fall into two broad categories. In the first category are those that enable direct connection to the QCD Lagrangian, such as Lattice QCD (LQCD) and QCD applications of the Dyson-Schwinger equations (DSE). In the second category are those that use models inspired by or derived from our knowledge of QCD, such as quark-hadron duality, light-front holographic QCD (AdS/QCD), light-cone sum rules (LCSR), and CQMs. It is important to realize that even those approaches that attempt to solve QCD directly can only do so approximately, and these approximations ultimately represent limitations that need careful consideration. As such, it is imperative that whenever possible the results of these intensive and challenging calculations be compared directly with the data from electroproduction experiments such as those from this current proposal. Comparisons of the experimental results to the theoretical predictions provide for crucial insights into many aspects of the dynamics, including confinement and DCSB, through mapping of the dressed quark mass function from the data on $\gamma_v NN^*$ electrocouplings, and from exploring manifestations of the non-perturbative strong interaction in the generation of excited states of different quantum numbers. It is the interplay between theory and experiment that leads to progress. Until exact calculations exist, approaches that model QCD will continue to have an important role to play.

In the last decade there has been marked progress in developing more realistic and more complete theoretical approaches. CQMs have been greatly refined by using fully relativistic treatments [3, 14] and by including sea quark components [15], and hypercentric CQMs with more proper treatment of constituent quark interactions [2] have been developed. In addition, a covariant model based on the Dyson-Schwinger equations [16, 17, 18] of QCD has

been shown to allow the baryon data to be interpreted directly in terms of current quarks and gluons. The DSE framework also provides an important link between the phenomenology of dressed current quarks and Lattice QCD [4]. Relations between baryon form factors and the Generalized Parton Distributions (GPDs) have also been developed that connect these two different approaches for describing baryon structure [19, 20]. On a fundamental level, LQCD is progressing rapidly toward making direct contact with the baryon data. Toward this end, the USQCD Collaboration [21] (which involves JLab's LQCD group) is working to perform calculations for predicting the baryon spectrum, as well as $\gamma_v NN^*$ transition form factors.

In the past decade the Excited Baryon Analysis Center (EBAC) at JLab made significant contributions to develop rigorous approaches to not only extract the N^* parameters from the available data, but also to develop a complete framework with which to interpret these data in terms of QCD-based approaches (CQMs, DSE, LQCD). A summary of the EBAC program (completed in 2012) is detailed in Ref. [4]. Looking toward the future, the Physics Analysis Center at JLab (established in 2013) is tasked specifically to work on amplitude analysis for various exclusive channels in order to further our knowledge on the N^* excitation spectrum and our understanding of N^* structure. In addition, the important work undertaken by the EBAC effort is being extended by the new Argonne-Osaka Collaboration [5], whose goal is to extend the analysis of meson production amplitudes through their dynamical coupled-channel approach to extract the mass, width, coupling constants, and electromagnetic transition form factors of the N^* states across the full resonance region. Ultimately the analysis of the full set of expected meson electroproduction data from CLAS12 will allow access to the dynamics of the non-perturbative strong interaction responsible for N^* formation. These analyses will be crucial for understanding the nature of confinement and dynamical chiral symmetry breaking in baryons.

This proposal will provide the necessary data from the exclusive KY channels on the Q^2 evolution of the transition form factors in the unexplored domain of $Q^2 > 5$ GeV^2. The experiment will also enable precision cross sections to be extracted in the range of Q^2 down to $\approx$1 GeV^2, which will be important to allow connection to the published CLAS KY data. For the foreseeable future, CLAS12 will be the only facility in the world capable of investigating the spectrum and the structure of excited nucleon states at distance scales where the quark degrees of freedom are expected to dominate. The extraction of the $\gamma_v NN^*$ transition amplitudes for the dominant N^* and Δ^* states from the comprehensive data based on this experiment, together with that provided by the already approved experiments of the 12 GeV program, will allow for the opportunity to better understand how the strong interaction of dressed quarks gives rise to the spectrum and structure of excited nucleon states, and how these states emerge from QCD.

2 N^* Program Objectives

The electrocoupling parameters determined from the data involving pionic channels for several low-lying N^* states for photon virtualities up to $Q^2 \sim 5$ GeV^2 has already provided valuable information (see Section 2.1). At these distance scales, the resonance structure is determined by both meson baryon dressing and dressed quark contributions. Here we propose to perform measurements that will allow for the determination of the Q^2 evolution of the corresponding electrocoupling parameters in the regime up to $Q^2 = 12$ GeV^2 for N^* states with masses in the range from 1.6 to 3 GeV using the exclusive $K^+\Lambda$ and $K^+\Sigma^0$ final states. Both channels will be measured simultaneously with the CLAS12 detector and an extensive database for N^* studies will be created from the proposed measurements that will extend and complement that expected from analysis of the single non-strange meson and $N\pi\pi$ channels of CLAS12 experiment E12-09-003 [11].

The full experimental program of N^* studies with the CLAS12 detector has a number of important objectives. These include:

i). To map out the quark structure of the dominant N^* and Δ^* states from the data acquired for meson electroproduction through the exclusive final states including $p\pi^0$, $n\pi^+$, $p\eta$, $p\omega$, $p\pi^+\pi^-$, $K^+\Lambda$, and $K^+\Sigma^0$. This objective is motivated by results from existing analyses such as those shown in Fig. 2, where it is seen that the meson-baryon dressing contribution to the N^* structure decreases rapidly with increasing Q^2. The data can be described approximately in terms of dressed quarks already for $Q^2 \sim 5$ GeV^2. It is therefore expected that the data at $Q^2 > 5$ GeV^2 can be used more directly to probe the quark substructure of the N^* and Δ^* states. The comparison of the extracted resonance electrocoupling parameters from this new higher Q^2 regime to the predictions from LQCD and DSE calculations will allow for a much improved understanding of how the internal dressed quark core emerges from QCD and how the dynamics of the strong interaction are responsible for the formation of the N^* and Δ^* states of different quantum numbers.

ii). To investigate the dynamics of dressed quark interactions and how they emerge from QCD. This work is motivated by recent developments of hadronic models based on the DSE approach, which has provided links between the dressed quark propagator, the dressed quark scattering amplitudes, and the QCD Lagrangian. DSE analyses of the extracted N^* electrocoupling parameters have the potential to allow for investigation of the origin of dressed quark confinement in baryons and the nature of DCSB, since both of these phenomena are rigorously incorporated into DSE approaches [4].

iii). To study the Q^2-dependence of the non-perturbative dynamics of QCD. This is motivated by studies of the momentum dependence of the dressed quark mass function of the quark propagator within LQCD [22] and DSE [16, 17]. The calculated mass function approaches the current quark mass of a few MeV only in the high Q^2 regime of perturbative QCD. However, for decreasing momenta, the current quark acquires a constituent mass of 300 MeV as it is dressed by quarks and gluons. Verification of this momentum dependence would further advance understanding of non-perturbative dynamics. Efforts are currently underway to study the sensitivity of the proposed transition form factor measurements to different parameterizations of the momentum dependence of the quark mass [23].

The data expected from the experiments of the CLAS12 N^* program will make possible the study of the kinematic regime of quark momenta $0.5 < p < 1.1$ GeV (where $p = \sqrt{Q^2}/3$), running over the dressed-quark propagator. The $\gamma_v NN^*$ electrocouplings will be sensitive to the transition from the confinement regime of strongly bound dressed quarks and gluons at small momenta, $p < 0.5$ GeV, to the pQCD regime for $p > 2$ GeV, where almost undressed and weakly interacting current quarks and gluons gradually emerge as the relevant degrees of freedom in resonance structure with increasing Q^2. The momentum dependence of the dressed-quark mass should affect all dressed-quark propagators and, therefore, the Q^2 evolution of the $\gamma_v NN^*$ electrocouplings. The dressed-quark dynamical structure and its mass function should be independent of the excited state quantum numbers. Therefore, the combined analyses of the data on electrocouplings of several prominent N^* states as seen through multiple final states should considerably improve our knowledge of the momentum dependence of dressed-quark masses and their dynamical structure.

iv). To offer constraints from resonance transition form factors for the $N \to N^*$ GPDs. We note that a key aspect of the CLAS12 measurement program is the characterization of exclusive reactions at high Q^2 in terms of GPDs. The elastic and $\gamma_v NN^*$ transition form factors represent the first moments of the GPDs [24, 25, 26], and they provide for unique constraints on the structure of nucleons and their excited states. Thus the N^* program at high Q^2 represents the initial step in a reliable parameterization of the transition $N \to N^*$ GPDs and is an important part of the larger overall CLAS12 program studying exclusive reactions.

This set of objectives was first laid out in the experimental proposal for E12-09-003 [11]. It was further updated and expanded upon in Ref. [4]. The addition of the measurements from the $K^+\Lambda$ and $K^+\Sigma^0$ final states serves to further expand and complement the already existing N^* program for CLAS12. In addition to these mainstream objectives, another almost tacit program objective is the study of the properties of the N^* and Δ^* states for the purpose of characterizing the nature of these states as conventional q^3 states or in terms of a possible q^3G configuration. This objective is discussed in Section 2.2.

2.1 N^* Studies in Meson Electroproduction with CLAS

The comprehensive experimental data sets obtained with the CLAS detector on single pseudoscalar meson electroproduction, e.g. $p\pi^0$, $n\pi^+$, $p\eta$, and KY, and double charged pion electroproduction, open up important new opportunities for measurements of the $\gamma_v NN^*$ transition helicity amplitudes (i.e. the N^* electrocoupling parameters) [27, 28]. The existing CLAS data provides extensive precision data for these exclusive channels, including differential cross sections and both single and double polarization observables, over a broad kinematic range from $Q^2 = 0.2$ to 4.5 GeV^2. Ultimately, these data make it possible to utilize well-established constraints from dispersion relations and to apply and develop phenomenological approaches for the Q^2 evaluation of the N^* electrocoupling parameters by fitting them to all available observables in a combined coupled-channel approach.

Several phenomenological analyses of the experimental data that have already been carried out within the CLAS Collaboration [4, 29, 30, 31, 32] have allowed for the determination of the transition helicity amplitudes for a variety of low-lying states: $P_{33}(1232)$, $P_{11}(1440)$,

$D_{13}(1520)$, $S_{11}(1535)$ (for example, see Figs. 2, 5, and 6). The analysis of the CLAS $N\pi\pi$ data allowed for the first mapping of the Q^2 evolution of the electrocoupling parameters for resonances with masses above 1.6 GeV: $S_{31}(1620)$, $D_{33}(1700)$, and $P_{13}(1720)$ [4, 8] (for example, see Fig. 7). In addition, the CLAS data on single-pion exclusive electroproduction were also analyzed within the framework of the MAID [33] and the SAID [34, 35] approaches. These reaction models have allowed access to the resonant amplitudes by fitting all available observables in each channel independently and within the framework of different reaction models.

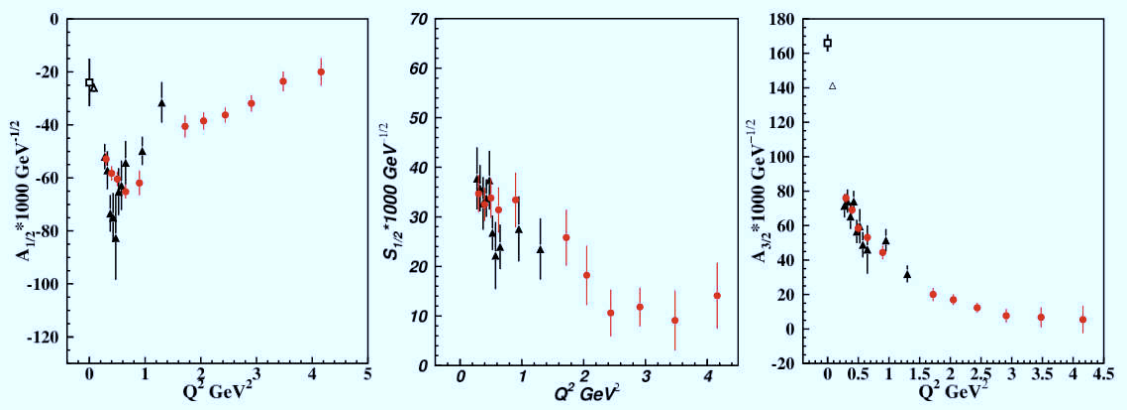

Figure 5: Electrocoupling parameters determined for the $D_{13}(1520)$ based on independent analysis of the CLAS $N\pi$ (circles) and $N\pi\pi$ (triangles) data [4]. The squares and triangles at $Q^2 = 0$ are from existing photoproduction data.

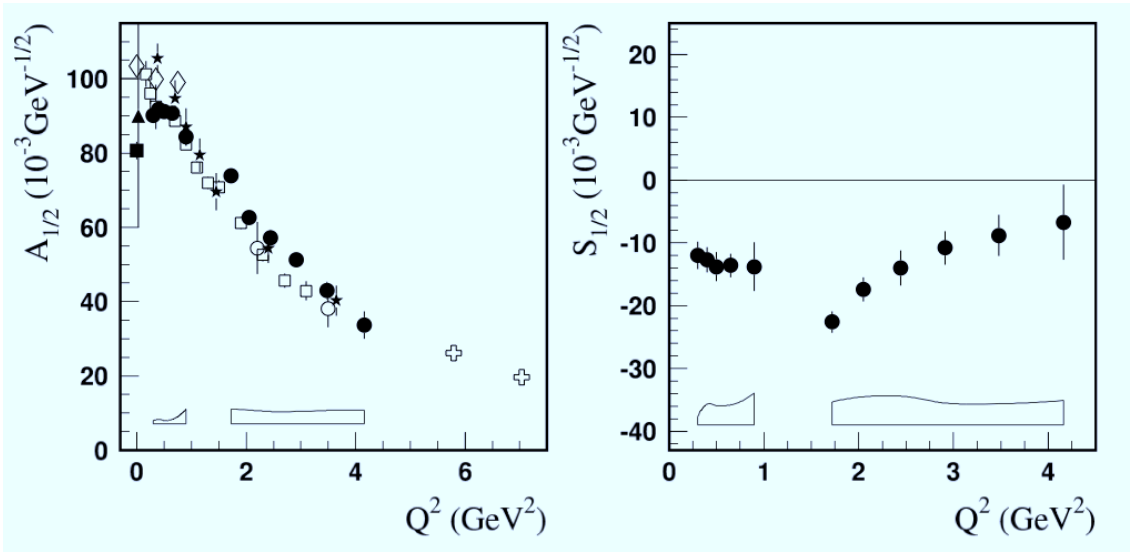

Figure 6: Electrocoupling parameters determined for the $S_{11}(1535)$. The full circles are based on analysis of the CLAS $N\pi$ data. The other data points are mainly based on independent analysis of CLAS $N\eta$ data [4]. Fit uncertainty bands are included at the bottom of each plot.

However, reliable extraction of the electrocouplings for these states must be supported by independent analyses of other exclusive electroproduction channels having different non-resonant mechanisms. The $K^+\Lambda$ and $K^+\Sigma^0$ electroproduction channels are expected to

provide valuable information to improve our knowledge on electrocouplings of the isospin-1/2 $P_{13}(1720)$ state due to isospin filtering in these exclusive channels. The studies of $K^+\Sigma^0$ electroproduction may further offer access to the electrocouplings of the $D_{33}(1700)$ and $F_{35}(1905)$ resonances. More detailed studies on the feasibility of incorporating these additional exclusive channels for evaluating the electrocouplings of high-lying resonances are, in any case, a clear and present need. Work to incorporate the existing CLAS $K^+\Lambda$ and $K^+\Sigma^0$ data into these existing approaches is now being organized. The veracity of the extracted electrocoupling parameters therefore relies on consistency of the results from analysis of multiple reaction channels.

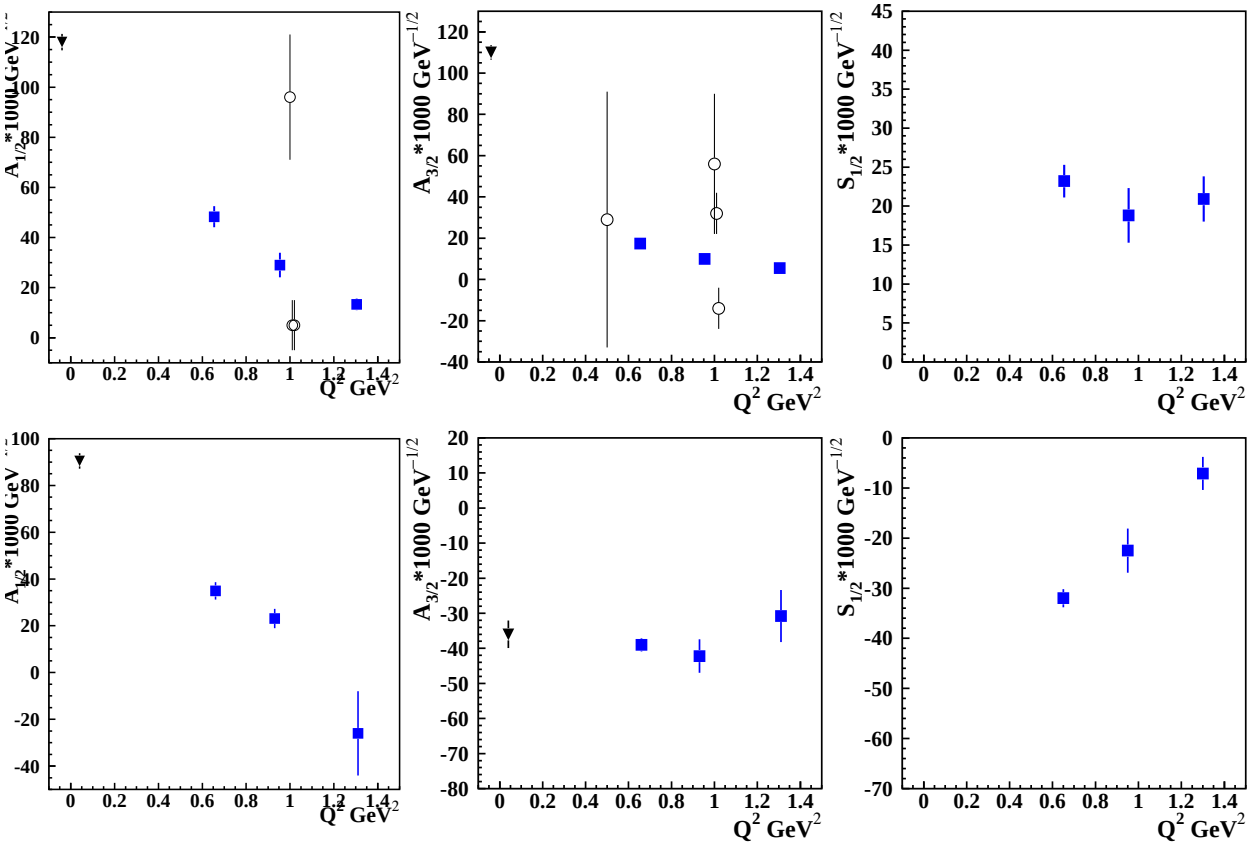

Figure 7: Electrocoupling parameters ($A_{1/2}$ (left), $A_{3/2}$ (center), $S_{1/2}$ (right)) determined for the $D_{33}(1700)$ (top) and $P_{13}(1720)$ (bottom) from Ref. [8]. The solid squares are data from the CLAS $N\pi^+\pi^-$ analysis, the triangles at Q^2=0 are from the CLAS photoproduction analysis of Ref. [36]. All other data points are taken from Ref. [37].

In order to determine the N^* electrocoupling parameters, a reliable separation of the resonant and non-resonant parts contributing to the production amplitudes is required. This is one of the most challenging aspects of the extraction procedure. So far, no approach based on a fundamental theory has been developed that would allow either a description of an effective meson-baryon Lagrangian or a selection of the contributing meson-baryon mechanisms. Therefore fits to the experimental data of various meson electroproduction channels must be employed to develop phenomenological reaction models that contain the relevant resonant and non-resonant mechanisms [4].

It is also important to note that the $N\pi$ and $N\pi\pi$ electroproduction channels represent

the two dominating exclusive channels in the resonance region. The knowledge of the electroproduction mechanisms for these channels is critically important for N^* studies in channels with smaller cross sections such as $K^+\Lambda$ and $K^+\Sigma^0$ production, as they can be significantly affected in leading order by coupled-channel effects produced by their hadronic interactions in the pionic channels.

2.2 Characterization of Hybrid Baryons

N^* and Δ^* states with valence gluons, or hybrid baryon states, are expected to exist if QCD is the correct theory of strong interactions. In fact, any model of QCD bound states that allows the gluon fields to be dynamical degrees of freedom will give rise to additional states that involve excitations of these degrees of freedom. A clear experimental signature of a hybrid N^* or Δ^* state does not exist as of yet, but evidence of such a state would be very important in understanding the strong interaction in QCD.

Hybrid baryons actually turn out to be a bit of a tricky issue to search for experimentally. This is because all spin/parity values that can be populated by such q^3G states can also be populated by ordinary q^3 states having excitation in the orbital angular momentum. Therefore, there are no "exotic" quantum numbers associated with hybrid baryons such as are possible for $q\bar{q}G$ mesons that can be used as an experimental tag.

With these considerations in mind, two approaches to an investigation of gluonic degrees of freedom to baryon spectra are possible. The first approach amounts to a detailed bookkeeping study where one attempts to establish whether there is evidence for more states in the spectrum than are predicted by the q^3 quark model alone. Ultimately, this approach is only truly viable in conjunction with detailed studies to establish the complete conventional q^3 baryon spectrum. What amounts to an unusual state might only be apparent once the set of conventional states is well understood, including their mass, decay width, and quantum numbers. Such an exercise certainly requires careful multi-channel analysis of reactions involving many different initial and final states.

The second approach to studying the N^* and Δ^* spectra for evidence of the presence of hybrid states involves a study of the Q^2 evolution of the electromagnetic production amplitudes that might be expected to be distinguishable for q^3G states relative to conventional q^3 states. Note that a complete description of the spectrum and the strong decays of the hybrid baryons must ultimately account for the degree of mixing between the q^3 and q^3G states. However, much can be learned about the N^* and Δ^* spectra by studying the production amplitudes as a function of Q^2. For example, Ref. [38] shows that in the domain of perturbative QCD, electroproduction of q^3G baryons will fall relative to background at high Q^2. However, for conventional q^3 baryons, the resonance peak to background ratio is constant with Q^2. These expectations follow from QCD counting rules for the asymptotic behavior of the form factors, where the form factor for a conventional baryon should fall off as $1/Q^3$, but a hybrid should fall off as $1/Q^5$. Thus studies of the electrocoupling parameters scaled by Q^3 might potentially reveal states with a non-conventional makeup. Figure 8 shows the Q^2 evolution of the $A_{1/2}$ electrocouplings of several conventional q^3 N^* states scaled by Q^3. A hybrid signature might be indicated by a state that showed a different scaling trend, indicative of a different constituent counting.

Of course, signatures of hybrid baryons will require careful experimental study and the-

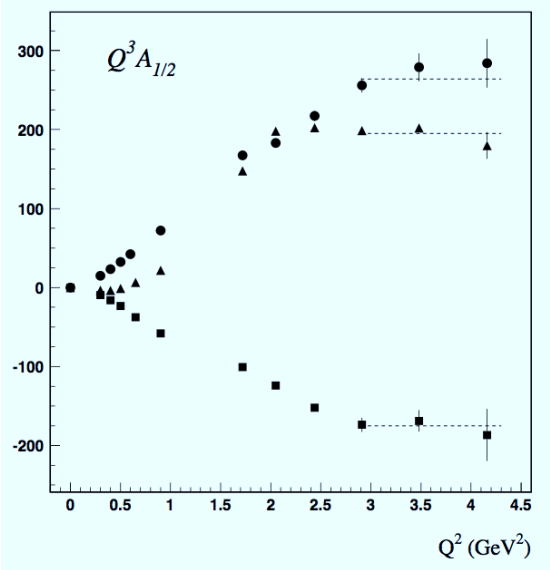

Figure 8: The $A_{1/2}$ electrocouplings of conventional q^3 N^* states $P_{11}(1440)$ (triangles), $D_{13}(1520)$ (squares), and $S_{11}(1535)$ (circles) scaled by Q^3 from analysis of CLAS data [7]. The horizontal dashed lines at high Q^2 are the expectations of scaling for these conventional baryon states from constituent counting rules derived from pQCD.

oretical modeling. For more than 20 years there were expectations that the $P_{11}(1440)$ could possibly be a hybrid state (e.g. see Refs. [39, 40]). However, today it has been accepted that this state has a behavior fully consistent with a radial excitation [4, 41]. Figure 9 shows the corresponding electrocoupling amplitudes compared to calculations for relativistic light front quark models and a model including an explicit gluonic contribution, which clearly is ruled out by the data.

Historically, most investigations of hybrid baryons have been carried out using the bag model [44]. Such calculations estimated the mass of the lowest hybrid state at ∼1.5 GeV. A similar mass estimate was obtained using a QCD sum rule calculation [45]. A calculation using a flux tube model gave a mass scale for the lowest q^3G state of ∼1.9 GeV [46]. Recently the first comprehensive study of hybrid baryons using LQCD (with $m_\pi = 400$ MeV) [47] showed that the lowest lying states having significant overlap onto the hybrid operators first appear at ∼1.3 GeV above the proton for the positive-parity states (see Fig. 10). The lowest lying LQCD hybrid states of negative parity lie somewhat higher in mass. A more complete understanding of the expected hybrid N^* and Δ^* states will require calculations at a more physical pion mass, as well as with calculations employing larger lattice volumes and smaller spacings. Significant progress is expected on this front on a timeline consistent with the data analysis for this experiment.

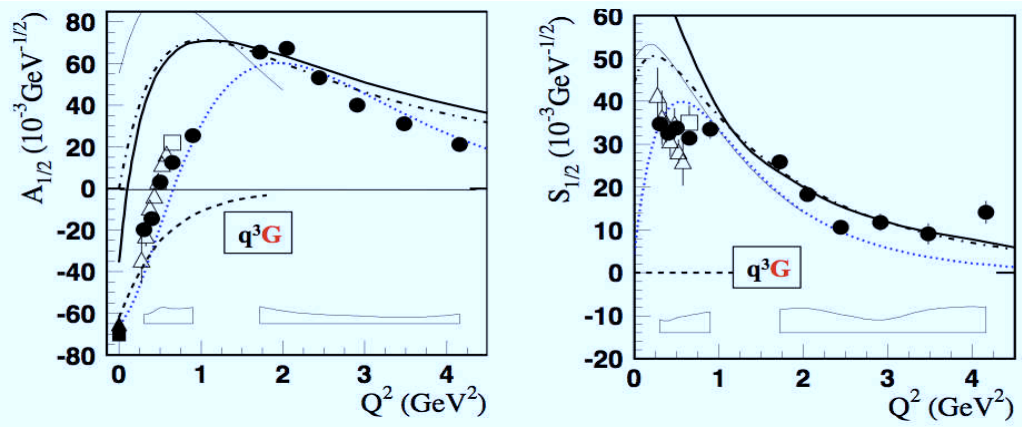

Figure 9: Electrocoupling amplitudes for the Roper $P_{11}(1440)$. The solid data points are from fits to CLAS $N\pi$ data [7], the open boxes are from a combined analysis of CLAS $N\pi$ and $N\pi\pi$ data [30], and the open triangles are from an analysis of CLAS $N\pi\pi$ data [42]. The thin solid curve is from a non-relativistic quark model and the other unlabeled curves are different quark model calculations. The blue dotted line is from the MAID2007 global analysis (see Ref. [28] for details). The thin dashed line labeled "q^3G" is for a gluonic excitation [43]. Fit uncertainty bands are included at the bottom of each plot.

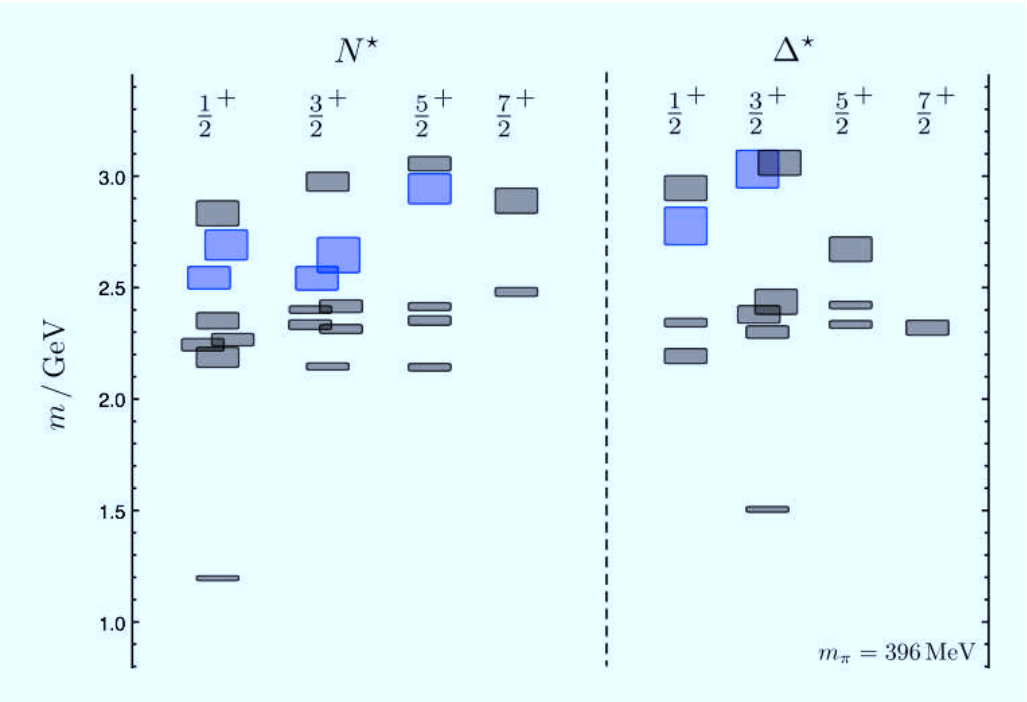

Figure 10: Spectrum of N^* and Δ^* states from LQCD calculations [47]. The gray boxes are the conventional qqq states and the blue boxes are the hybrid states.

3 Exclusive KY Final States

3.1 $N^*, \Delta^* \to KY$ Coupling

The flavor structure of baryons and their resonances is well described in quark models that assume a basis built up from three constituent quarks. The spatial and spin-orbit wavefunctions can be described using a confinement potential with residual interactions between the constituent quarks. A common feature of the models is that the dynamics of three quarks leads to a spectrum of states much more numerous than has been confirmed experimentally. This discrepancy has been the seed for the development of models derived from an altered quark basis. One of the most prevalent considers baryons as made of a quark and di-quark. This has led to much discussion that has not yet been fully resolved [48, 49, 50, 51]. One model prediction of the N^* and Δ^* spectrum derived from a quark-diquark basis showed a reasonable match to the experimental excitation spectrum, provided only three- and four-star PDG rated states were considered [52].

Even today, much of what we know about the states in the N^* and Δ^* spectra was derived from data involving pion-nucleon elastic scattering. However, if a resonance couples weakly to these channels, it could have been missed in the data. This could explain the issues with the long-standing missing resonance problem. This reasoning provided a strong motivation for the CLAS N^* program studying photo- and electroproduction of s-channel baryon resonances decaying to a host of meson-baryon final states. Certainly the high-statistics data sets of exclusive $N\pi$ and $N\pi\pi$ final states have proven especially important in studies of the N^* spectrum [4, 7, 26, 31, 32].

However, it has also been the case that unique and critical insight into the N^* and Δ^* excitation spectra has been provided through the photo- and electroproduction of both the $K^+\Lambda$ and $K^+\Sigma^0$ final states. These final states, due to the creation of an $s\bar{s}$ quark pair in the intermediate state, are naturally sensitive to coupling to high-lying s-channel resonance states at $W > 1.6$ GeV. Note also that although the two ground-state hyperons have the same valence quark structure (uds), they differ in isospin, such that intermediate N^* resonances can decay strongly to $K^+\Lambda$ final states, but intermediate Δ^* states cannot. Because $K^+\Sigma^0$ final states can have contributions from both N^* and Δ^* states, the hyperon final state selection constitutes an isospin filter.

To date the PDG lists only four N^* states, $S_{11}(1650)$, $P_{11}(1710)$, $P_{13}(1720)$, and $P_{13}(1900)$, with known couplings to $K\Lambda$ and no N^* states are listed that couple to $K\Sigma$ [13]; only a single Δ^* state, $P_{33}(1920)$, is listed with coupling strength to $K\Sigma$ (see Table 1). The branching ratios to KY provided for these states are typically less than 10% with uncertainties of the size of the measured coupling. While the relevance of this core set of N^* states in the $\gamma^{(*)}p \to K^+\Lambda$ reaction has long been considered a well-established fact, this set of states falls short of reproducing the experimental results for $W < 2$ GeV, and several analyses [53, 54] have called the importance of the $P_{11}(1710)$ state into question.

Beyond the core set of N^* states, the PDG lists the $P_{13}(1900)$ state as the sole established N^* near 1900 MeV. However, with a 500-MeV width quoted by some measurements, it is unlikely that this state by itself can explain the $K^+\Lambda$ cross sections for $W < 2$ GeV, unless its parameters are significantly different than those given by the PDG. Several analyses [55, 56] have shown this state (with $M = 1915 \pm 60$ MeV and $\Gamma = 180 \pm 40$ MeV) to be necessary to describe the CLAS beam-recoil polarization data [57]. Note that the $P_{13}(1900)$ state is

predicted by symmetric quark models and its existence is not expected in diquark models. In the recent fits of $\gamma p \to K^+\Sigma^0$ data, all N^* resonances found to be necessary to fit the $K^+\Lambda$ data have been included. However, the existing $K^+\Sigma^0$ database is smaller than the $K^+\Lambda$ database, with notably larger statistical uncertainties.

$N^* \to KY$				$\Delta^* \to K\Sigma$		
State	Rating	B.R. ($K\Lambda$)	B.R. ($K\Sigma$)	State	Rating	B.R. ($K\Sigma$)
$N^*(1650)S_{11}$	****	3 - 11%	–	$\Delta^*(1700)D_{33}$	****	–
$N^*(1675)D_{15}$	****	$< 1\%$	–	$\Delta^*(1750)P_{31}$	*	–
$N^*(1680)F_{15}$	****	–	–	$\Delta^*(1900)S_{31}$	**	–
$N^*(1700)D_{13}$	***	$< 3\%$	–	$\Delta^*(1905)F_{35}$	****	–
$N^*(1710)P_{11}$	***	5 - 25%	–	$\Delta^*(1910)P_{31}$	****	–
$N^*(1720)P_{13}$	***	1 - 15%	–	$\Delta^*(1920)P_{33}$	***	2.1%
$N^*(1900)P_{13}$	**	0 - 10%	–	$\Delta^*(1930)D_{35}$	***	–
$N^*(1990)F_{17}$	**	–	–	$\Delta^*(1940)D_{33}$	*	–
$N^*(2000)F_{15}$	**	–	–	$\Delta^*(1950)F_{37}$	****	–
				$\Delta^*(2000)F_{35}$	**	–

Table 1: Listing of the N^* couplings to KY and the Δ^* couplings to $K\Sigma$ for states below $W = 2$ GeV from the 2012 PDG listings [13].

A recent development in understanding the N^* spectrum was provided by the Bonn-Gatchina coupled-channel partial wave analysis of the hadronic $N\pi$ and the photoproduced γp channels [58]. This work presents an up-to-date listing of pole parameters and branching fractions for all N^* and Δ^* states up to $\sim$2 GeV with uncertainties at the level of a few percent (see Table 2). That analysis provided a list of (i) six N^* states with coupling to $K\Lambda$, $S_{11}(1650)$, $P_{11}(1710)$, $P_{13}(1895)$, $P_{11}(1880)$, $S_{11}(1895)$, and $P_{13}(1900)$, (ii) five N^* states with coupling to $K\Sigma$, $D_{13}(1875)$, $P_{11}(1880)$, $S_{11}(1895)$, $P_{13}(1900)$, and $D_{15}(2060)$, and (iii) four Δ^* states with coupling to $K\Sigma$, $S_{31}(1900)$, $P_{31}(1910)$, $P_{33}(1920)$, and $F_{37}(1950)$. For more on this list of states that couple to $K\Lambda$ and $K\Sigma$, see Ref. [59].

The findings of Ref. [58] are based on a significant amount of precision experimental data and a sophisticated coupled-channel fitting algorithm. However, in general, the issue of how to extract nucleon resonance content from open strangeness reactions is a long-standing question. Various analyses have led to very different conclusions concerning the set of resonances that contribute (e.g. compare results from Refs. [56], [60], and [61], as well as the statements made regarding the resonant set from Ref. [58]). Furthermore, lack of sufficient experimental information, incomplete kinematic coverage, and underestimated systematics are still responsible for inconsistencies among the different models that fit the data to extract the contributing resonances and their properties [61, 62].

The indeterminacy for the open strangeness channels is in contrast to the pionic channels, where the contributing resonances can be more reliably identified by means of a partial wave analysis for $W < 2$ GeV. In open strangeness channels, this technique is less powerful as the non-resonant background contributions are a much larger fraction of the overall response. Several groups have stressed that the importance of the background contributions in the KY channels calls for a framework that accounts for both the resonant and non-resonant processes

$N^* \to KY$				$\Delta^* \to K\Sigma$		
State	Rating	B.R. ($K\Lambda$)	B.R. ($K\Sigma$)	State	Rating	B.R. ($K\Sigma$)
$N^*(1650)S_{11}$	****	10±5%	–	$\Delta^*(1620)S_{31}$	****	–
$N^*(1675)D_{15}$	****	–	–	$\Delta^*(1700)D_{33}$	****	–
$N^*(1680)F_{15}$	****	–	–	$\Delta^*(1750)P_{31}$	*	–
$N^*(1700)D_{13}$	***	–	–	$\Delta^*(1900)S_{31}$	**	5±3%
$N^*(1710)P_{11}$	***	23±7%	–	$\Delta^*(1905)F_{35}$	****	–
$N^*(1720)P_{13}$	****	–	–	$\Delta^*(1910)P_{31}$	****	9±5%
$N^*(1875)D_{13}$	***	4±2%	15±8%	$\Delta^*(1920)P_{33}$	***	4±2%
$N^*(1880)P_{11}$	**	2±1%	17±7%	$\Delta^*(1930)D_{35}$	***	–
$N^*(1895)S_{11}$	**	18±5%	13±7%	$\Delta^*(1940)D_{33}$	***	–
$N^*(1900)P_{13}$	**	16±5%	5±2%	$\Delta^*(1950)F_{37}$	****	0.4±0.1%
$N^*(1990)F_{17}$	**	–	–	$\Delta^*(2000)F_{35}$	**	–
$N^*(2000)F_{15}$	**	–	–			
$N^*(2060)D_{15}$	***	–	3±2%			

Table 2: Findings from the Bonn-Gatchina coupled-channel model for N^* couplings to KY and Δ^* couplings to $K\Sigma$ for states below $W \approx 2$ GeV [58].

and that provides for a means to constrain both of these classes of reaction mechanisms independently [63, 64].

At this point the lion's share of attention on the strangeness channels from CLAS has been given to the high-precision photoproduction data sets [57, 65, 66, 67]. One very important result from the CLAS $\gamma p \to K^+\Lambda$ data was the strong evidence for the $P_{13}(1900)$ state from fits that included the differential cross sections and the beam-recoil transferred polarization observables C_x and C_z [56] (see Fig. 11). This type of analysis clearly demonstrates the critical importance of studying not only the dominant $N\pi$ and $N\pi\pi$ channels, but also channels involving KY final states as well. At the current time, the $P_{13}(1900)$ state is ready for promotion from a 2-start to a 4-star PDG assignment and is set to become the first baryon resonance observed and confirmed in electromagnetic meson production, specifically due to the constraints provided by the $K^+\Lambda$ observables.

3.2 KY Electroproduction

In kaon electroproduction a beam of electrons with four-momentum $p_e = (E_e, \vec{p}_e\,)$ is incident upon a fixed proton target of mass M_p, and the outgoing scattered electron with momentum $p_{e'} = (E_{e'}, \vec{p}_{e'}\,)$ and kaon with momentum $p_K = (E_K, \vec{p}_K)$ are measured. The cross section for the exclusive K^+Y final states is then differential in the scattered electron momentum and kaon direction. Under the assumption of single-photon exchange, where the virtual photon has four-momentum $q = p_e - p_{e'} = (\nu, \vec{q}\,)$, this can be expressed as the product of an equivalent flux of virtual photons and the $\gamma^* p$ center-of-mass (CM) virtual photoabsorption cross section as:

$$\frac{d^5\sigma}{dE_{e'}d\Omega_{e'}d\Omega_K^*} = \Gamma\frac{d^2\sigma_v}{d\Omega_K^*}, \tag{1}$$

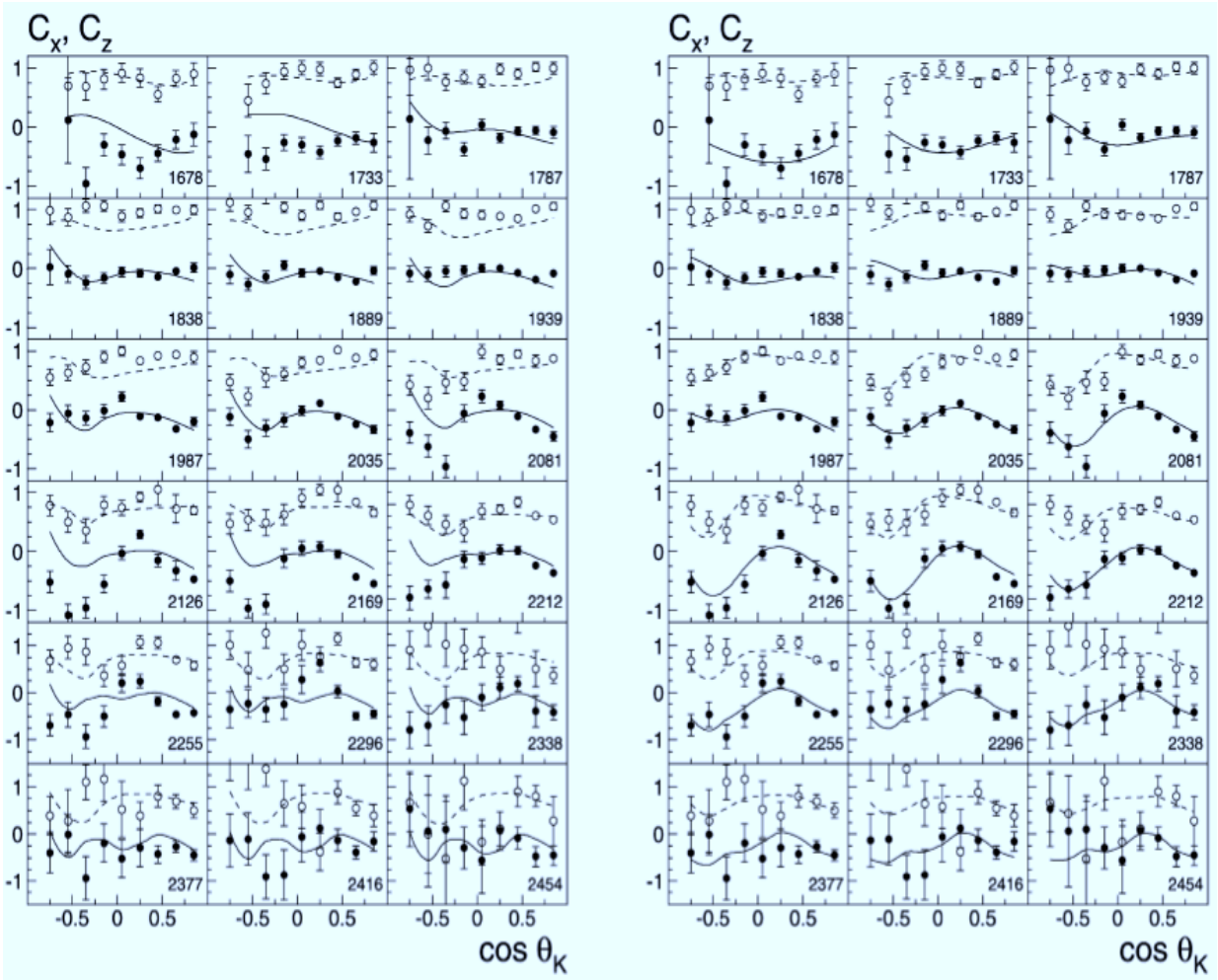

Figure 11: CLAS photoproduction $K^+\Lambda$ beam-recoil polarization transfer observables C_x (solid circles) and C_z (open circles) as a function of $\cos\theta^*_K$. The solid and dashed curves are from the partial wave analysis of Ref. [56] obtained without (left panel) and with (right panel) the $P_{13}(1900)$ state included in the fit. Each subplot is labeled with its associated W value in MeV.

where the virtual photon flux factor Γ depends only upon the electron scattering process. After integrating over the azimuthal angle of the scattered electron, the photoabsorption cross section can be expressed in terms of the variables Q^2, W, θ_K^*, and Φ, where $Q^2 = -q^2$ is the squared four-momentum of the virtual photon, $W = \sqrt{M_p^2 + 2M_p\nu - Q^2}$ is the total energy in the CM frame, θ_K^* is the CM kaon angle relative to the virtual photon direction, and Φ is the angle between the leptonic and hadronic production planes. A schematic illustration of electron scattering off a proton target, producing a final state electron, K^+, and hyperon Y is shown in Fig. 12.

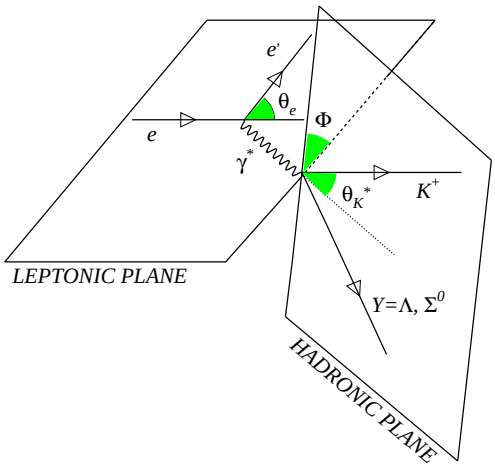

Figure 12: Kinematics in the laboratory frame for K^+Y electroproduction defining the angles θ_K^* and Φ.

Introducing the appropriate Jacobian, the form of the cross section can be rewritten as:

$$\frac{d^4\sigma}{dQ^2 dW d\Omega_K^*} = \Gamma_v \frac{d^2\sigma_v}{d\Omega_K^*}, \tag{2}$$

where

$$\Gamma_v = \frac{\alpha}{4\pi} \frac{W}{M_p^2 E^2} \frac{W^2 - M_p^2}{Q^2} \frac{1}{1-\epsilon} \tag{3}$$

is the flux of virtual photons (using the convention of Ref. [68]),

$$\epsilon = \left(1 + 2\frac{\nu^2}{Q^2} \tan^2 \frac{\theta_{e'}}{2}\right)^{-1} \tag{4}$$

is the polarization parameter of the virtual photon, and $\theta_{e'}$ is the electron polar scattering angle in the laboratory frame.

For the case of an unpolarized electron beam (helicity h=0) with no target or recoil polarizations, the virtual photon cross section can be written (using simplifying notation) as:

$$\frac{d\sigma}{d\Omega_K^*}(h=0) \equiv \sigma_0 = \sigma_T + \epsilon\sigma_L + \epsilon\sigma_{TT}\cos 2\Phi + \sqrt{\epsilon(1+\epsilon)}\sigma_{LT}\cos\Phi, \tag{5}$$

where σ_i are the structure functions that measure the response of the hadronic system and $i = T$, L, TT, and LT represent the transverse, longitudinal, and interference structure functions [69]. The structure functions are, in general, functions of Q^2, W, and θ_K^* only.

For the case of a polarized electron beam with helicity h, the cross section form of Eq.(5) is modified to include an additional term:

$$\frac{d\sigma}{d\Omega_K^*} = \sigma_0 + h\sqrt{\epsilon(1-\epsilon)}\sigma_{LT'}\sin\Phi. \tag{6}$$

The electron beam polarization produces a fifth structure function $\sigma_{LT'}$ that is related to the beam helicity asymmetry via:

$$A_{LT'} = \frac{\frac{d\sigma^+}{d\Omega_K^*} - \frac{d\sigma^-}{d\Omega_K^*}}{\frac{d\sigma^+}{d\Omega_K^*} + \frac{d\sigma^-}{d\Omega_K^*}} = \frac{\sqrt{\epsilon(1-\epsilon)}\sigma_{LT'}\sin\Phi}{\sigma_0}, \tag{7}$$

where the $\pm$ superscripts on $\frac{d\sigma}{d\Omega_K^*}$ correspond to the electron helicity states of $h = \pm 1$.

While there have been a number of publications of precision cross sections and spin observables for both the photo- and electroproduction reactions, the vast majority of the theoretical effort to date has focused on fitting just the photoproduction data. Although KY photoproduction is easier to treat theoretically than KY electroproduction, and is thus more amenable to a detailed quantitative analysis, the electroproduction reaction is potentially a much richer source of information concerning hadronic and electromagnetic interactions. Some of the most important aspects of electroproduction include:

- The data are sensitive to the internal structure of baryon resonances through the Q^2 dependence of the electromagnetic form factors of the intermediate hadronic resonances associated with the strangeness production mechanism [62, 64, 70, 71, 72].

- The structure functions are particularly powerful to gain control over the parameterization of the background diagrams [73].

- Studies of finite Q^2 processes are sensitive to both transverse and longitudinal virtual photon couplings, in contrast to the purely transverse response probed in photoproduction.

- The longitudinal/transverse interference structure functions provide signatures of interfering partial wave strengths that are often dramatic and have been shown to be useful for differentiating between models of the production amplitudes [63, 74, 75, 76, 77, 78].

- The beam-recoil transferred polarizations in the $K^+\Lambda$ and $K^+\Sigma^0$ reactions, as well as the recoil polarization in the $K^+\Lambda$ reaction, have been shown to provide important new constraints to models that describe the photoproduction data [61, 79, 80, 81].

The world's database for $K^+\Lambda$ and $K^+\Sigma^0$ electroproduction in the nucleon resonance region ($1.6 < W < 3.0$ GeV) in the domain of momentum transfer $0.5 < Q^2 < 4$ GeV^2 is completely dominated by the measurements of the CLAS program. These include measurements of beam-recoil transferred polarization [79, 80] and induced recoil polarization [81]. Also extensive measurements of the separated structure functions $\sigma_U = \sigma_T + \epsilon\sigma_L$, σ_{LT}, σ_{TT},

and $\sigma_{LT'}$ [74, 75, 77] have been published. Finally, the first Rosenbluth separation from CLAS data at beam energies of 2.5 and 4 GeV allowed for a separation of σ_T and σ_L [74, 82].

The most precise data on the separated structure functions from fits to the CLAS $K^+\Lambda$ and $K^+\Sigma^0$ differential cross sections were acquired at a beam energy of 5.5 GeV, W from threshold to 2.6 GeV, Q^2 from 1.4 to 3.9 GeV^2, and nearly the full center-of-mass angular range of the kaon [77]. The complete data (σ_U, σ_{LT}, σ_{TT}, and $\sigma_{LT'}$) for one of the published points at Q^2=1.80 GeV^2 are shown in Fig. 13 for $K^+\Lambda$ and Fig. 14 for $K^+\Sigma^0$. The following model curves are overlaid on the data:

- The hadrodynamic model of Maxwell *et al.* (MX) (red/dashed curves - thinner line type from Refs. [64, 83], thicker line type is an extension of the model including fits to the $\sigma_{LT'}$ data from Ref. [75]). Note that this model is only available for the $K^+\Lambda$ final state and calculations go to a maximum W of 2.275 GeV.

- The t-channel Regge background model of Guidal *et al.* (GLV) [84] (blue/dotted) that contains no s-channel resonance contributions.

- The Regge plus resonance model of Ghent (RPR) [63] (black/solid curves - RPR-2007 thinner line type, RPR-2011 thicker line type). For the $K^+\Sigma^0$ comparison, only the RPR-2007 version is presently available.

In general, none of the available models provides an adequate description of the structure functions measured in either $K^+\Lambda$ or $K^+\Sigma^0$ electroproduction. Of course the hadrodynamic models are a quite reasonable description of the photoproduction data as they were directly employed to fit the model parameters. Thus the electroproduction data provide the potential to gain new understanding on both the resonant and non-resonant processes contributing to the reaction mechanism for these final states. In terms of the resonant contributions, these data have the potential to provide new information on the parameters of the contributing N^* states as well as the contributing u-channel processes.

One of the essential requirements in order to reliably extract the electrocoupling parameters from the K^+Y structure function data is a reaction model that provides a fully accurate description of the data across its full kinematic extent. Clearly none of the available models is presently at this point. One important aspect of this work is the development of such a reaction model that can be employed in the description of the data for Q^2 up to 12 GeV^2 while spanning the full resonance region. This is discussed in further detail in Section 3.5.

The CLAS electroproduction data provides a large Q^2 reach over the range from which the dynamics are dominated by meson-baryon degrees of freedom to that in which the quark-gluon degrees of freedom are becoming manifest. The published data for σ_U at E_b=5.5 GeV are shown in Figs. 15 and 16 for the $K^+\Lambda$ and $K^+\Sigma^0$ final states at two representative W points, 1.725 and 1.925 GeV [77]. Included on these plots are the photoproduction differential cross sections for $K^+\Lambda$ from Ref. [66] and $K^+\Sigma^0$ from Ref. [67] at Q^2=0 for the kinematic points where they are available. Also shown are the data for σ_U from Ref. [74] from two different data sets, (i). E_b=2.567 GeV, Q^2=0.65, 1.0 GeV^2 and (ii). E_b=4.056 GeV, Q^2=1.0, 1.55, 2.05, 2.55 GeV^2, at kinematic points that are reasonably close to the present data. The goal from the current experimental proposal is to extend these measurements up to the highest Q^2 of 12 GeV^2, where the dynamics are dominated by the quark-gluon degrees of freedom.

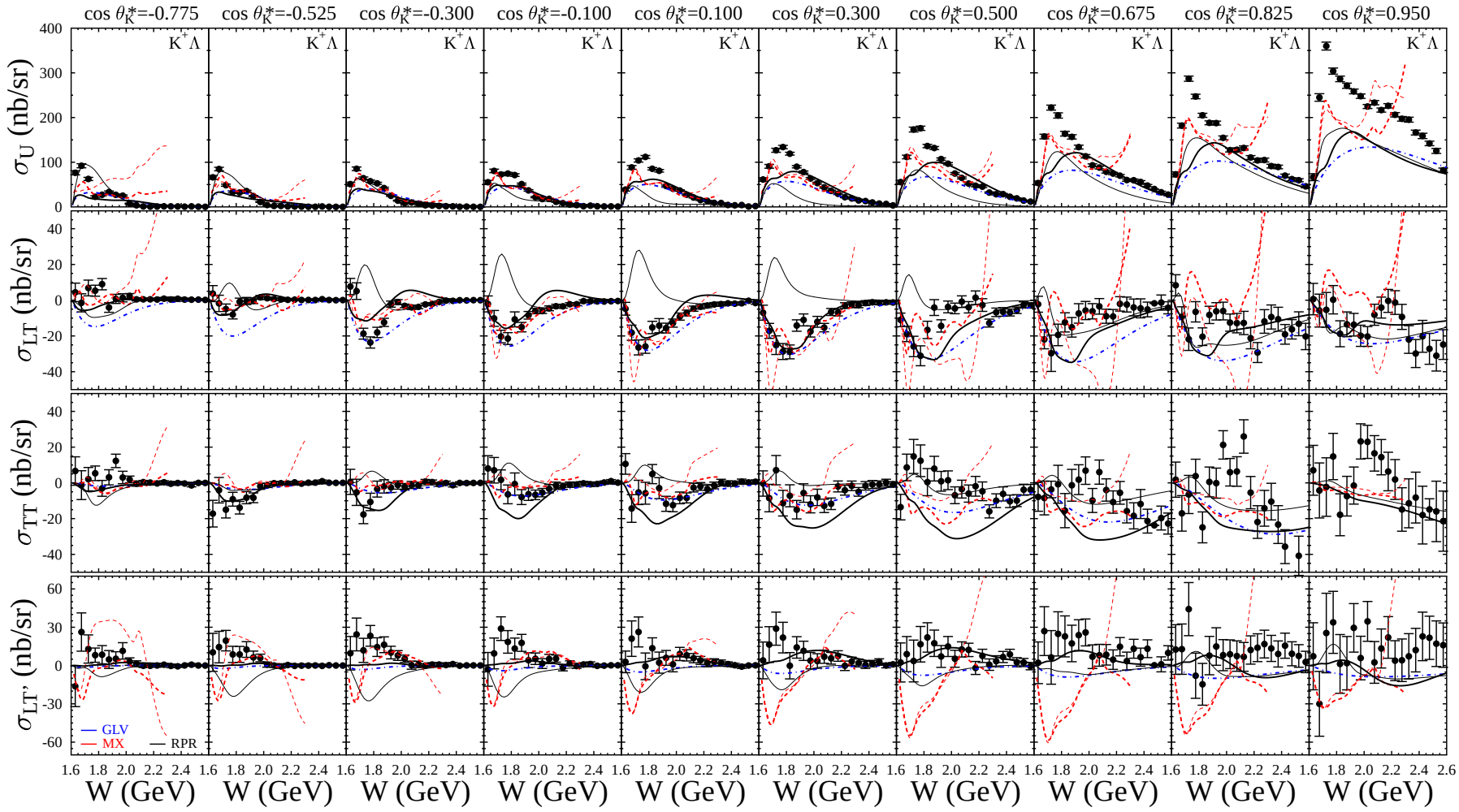

Figure 13: Structure functions $\sigma_U = \sigma_T + \epsilon\sigma_L$, σ_{LT}, σ_{TT}, and $\sigma_{LT'}$ (nb/sr) for $K^+\Lambda$ production vs. W at 5.5 GeV for Q^2=1.80 GeV^2 and $\cos\theta^*_K$ values as shown from CLAS data [77]. The error bars represent the statistical uncertainties only. The blue curves are from the GLV Regge model [84], the red curves are from the hadrodynamic model of Maxwell [64, 83], and the black curves are from the hybrid RPR model from Ghent [63]. See text for details.

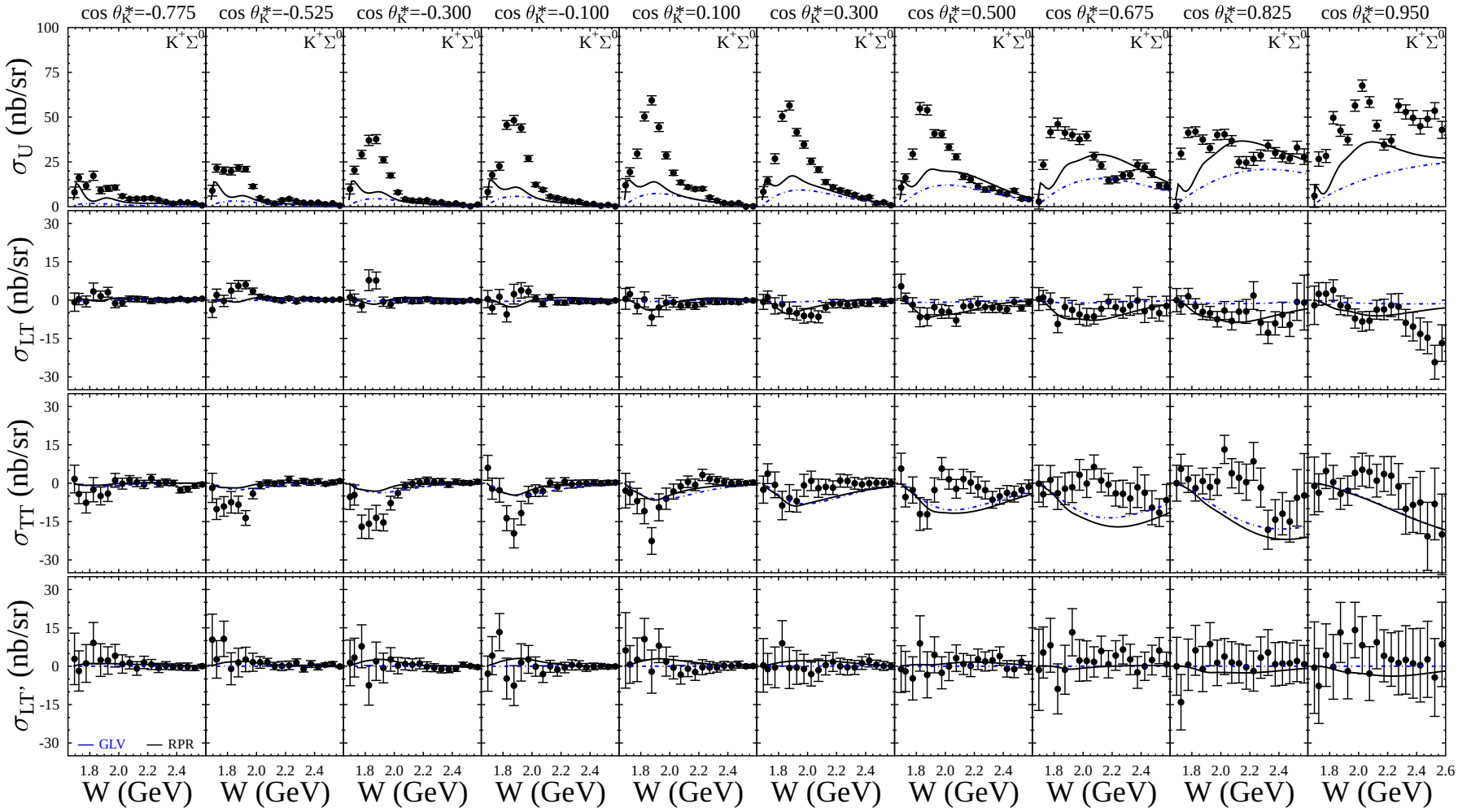

Figure 14: Structure functions $\sigma_U = \sigma_T + \epsilon\sigma_L$, σ_{LT}, σ_{TT}, and $\sigma_{LT'}$ (nb/sr) for $K^+\Sigma^0$ production vs. W at 5.5 GeV for Q^2=1.80 GeV^2 and $\cos\theta^*_K$ values as shown from CLAS data [77]. The error bars represent the statistical uncertainties only. The blue curves are from the GLV Regge model [84] and the black curves are from the hybrid RPR model from Ghent [63]. See text for details.

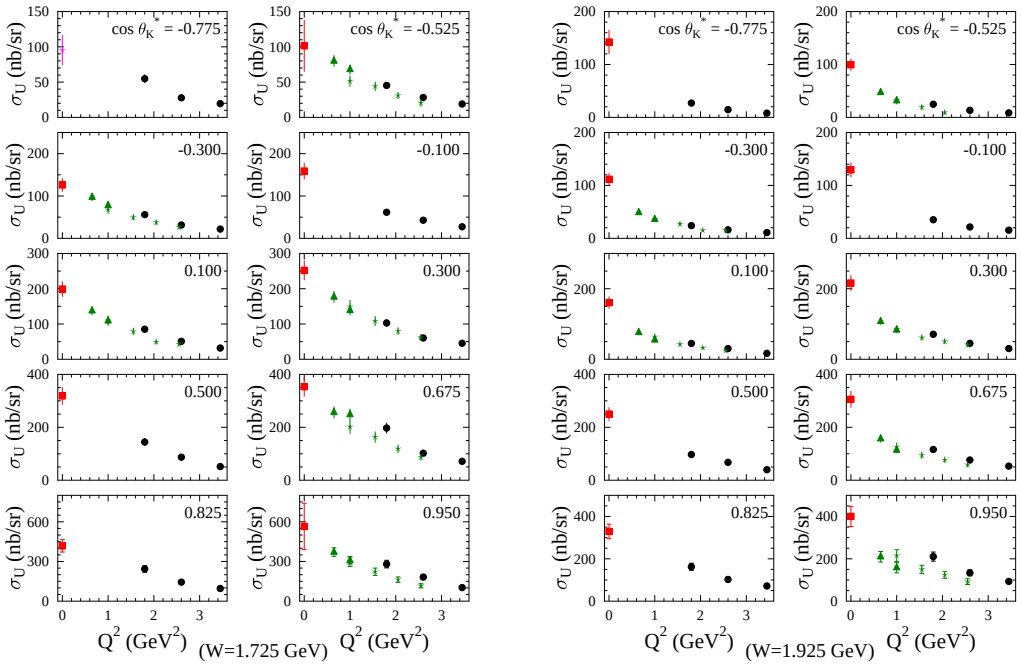

Figure 15: Structure function σ_U vs. Q^2 for the $K^+\Lambda$ final state for W=1.725 GeV (left) and 1.925 GeV (right) from CLAS data. The labels on each subplot indicate the $\cos\theta^*_K$ bin center. The black circles are the data from Ref. [77], the red squares are the photoproduction points from Ref. [66], and the green stars and triangles are from the lower Q^2 data from Ref. [74]. The error bars include both statistical and systematic uncertainties.

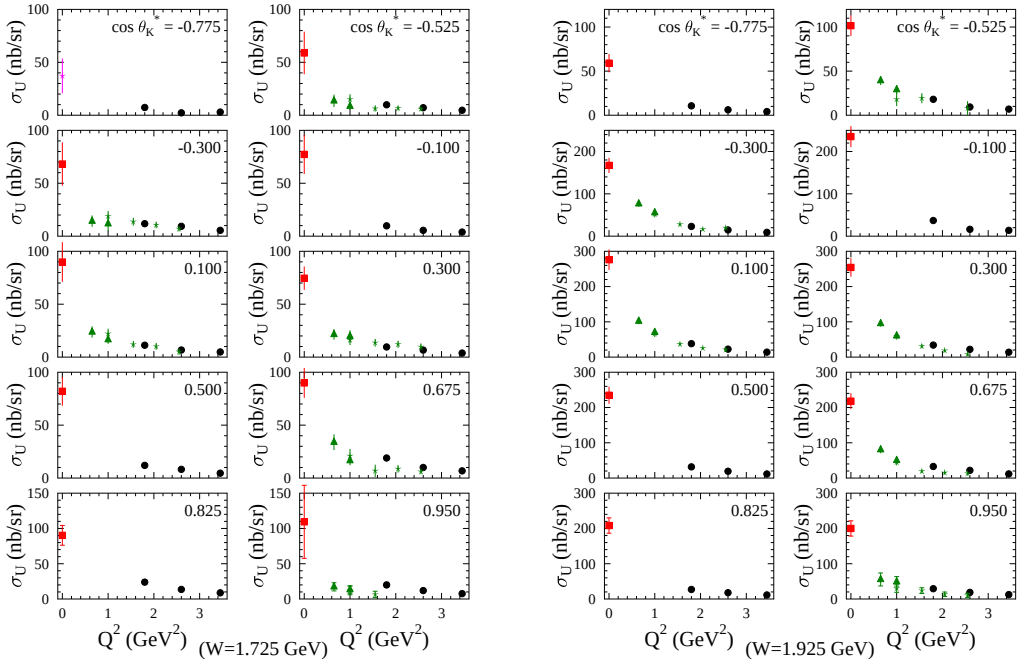

Figure 16: Structure function σ_U vs. Q^2 for the $K^+\Sigma^0$ final state for W=1.725 GeV (left) and 1.925 GeV (right) from CLAS data. The labels on each subplot indicate the $\cos\theta^*_K$ bin center. The black circles are the data from Ref. [77], the red squares are the photoproduction points from Ref. [67], and the green stars and triangles are from the lower Q^2 data from Ref. [74]. The error bars include both statistical and systematic uncertainties.

3.3 Electroproduction Analysis

During the past several years there has been much progress in extracting $\gamma_v NN^*$ transition form factors for several low-lying N^* states. These include the $P_{33}(1232)$, $P_{11}(1440)$, $D_{13}(1520)$, and $S_{11}(1535)$. The extraction of these electrocoupling parameters has relied mainly on fits to the CLAS $N\pi$ and $N\pi\pi$ channels obtained in the range $0.2 < Q^2 < 4.5$ GeV^2.

Nucleon resonances have various decay modes and hence manifest themselves through multiple final state channels. The contributions of the non-resonant amplitudes are substantially different in these different channels [27, 85]. However, it must be the case that the electrocoupling parameters for a given N^* state are independent of the decay channel as they are fully determined by the $\gamma_v NN^*$ vertices of the formation channel. The successful description of a large body of observables in various exclusive channels with a common set of N^* electrocoupling parameters gives strong evidence that the $\gamma_v NN^*$ helicity amplitudes can be reliably determined from different hadronic final states.

One of the key aspects of the analysis leading to the determination of the electrocoupling parameters for the $P_{11}(1440)$ and $D_{13}(1520)$ is the agreement of the results from the $N\pi$ and $N\pi\pi$ channels (see Figs. 2 and 5). Note, however, that the $N\pi$ channel is mostly sensitive to N^*s with masses lower than 1.6 GeV. One of the critical aspects of the KY channels is that they represent an independent final state with completely different non-resonant amplitudes relative to the pionic channels that will be extremely valuable in providing an independent cross-check of the $N\pi\pi$ analysis in the region of the high-lying resonances up to $W = 3$ GeV. In fact, the independent analysis of the separate KY and $N\pi\pi$ electroproduction channels offers the best opportunity for a detailed investigation of the structure of the dominant higher-lying resonances for $W > 1.6$ GeV.

The results obtained for the $N\pi$ and $N\pi\pi$ data already represent consistent initial estimates of the Q^2 evolution of the low-lying N^* electrocoupling parameters. This information will be checked and extended in a global and complete coupled-channels analysis of all major meson electroproduction channels including the KY data that incorporate the amplitudes of non-resonant electroproduction mechanisms extracted from the CLAS and CLAS12 data using the phenomenological approaches developed to study the data.

3.4 Legendre Fits

In order to investigate in a cursory manner the evidence for N^* resonance couplings in the separated structure functions for the CLAS data at $Q^2 < 4$ GeV^2, a series of Legendre polynomial fits was carried out [77]. The first approach fit the individual structure functions σ_U, σ_{LT}, σ_{TT}, and $\sigma_{LT'}$ versus $\cos\theta^*_K$ for each Q^2 and W point for the $K^+\Lambda$ and $K^+\Sigma^0$ final states using a truncated series of Legendre polynomials as:

$$C_{\ell=0\rightarrow 3} = \int_{-1}^{+1} \frac{d\sigma_{U,LT,TT,LT'}}{d\Omega^*} P_\ell(\cos\theta^*_K)\ d\cos\theta^*_K. \tag{8}$$

The fit coefficients for $\ell = 0 \rightarrow 3$ are shown for $K^+\Lambda$ in Fig. 17 and for $K^+\Sigma^0$ in Fig. 18 for $Q^2 = 1.80$ GeV^2. It is expected that the appearance of a structure in a single C_ℓ coefficient at the same W value and in each of the Q^2 points is likely a signal of an N^* contribution. Note that the appearance of a structure at a given value of W for each of the different C_ℓ

coefficients most likely suggests the presence of a dynamical effect rather than the signature of an N^* contribution.

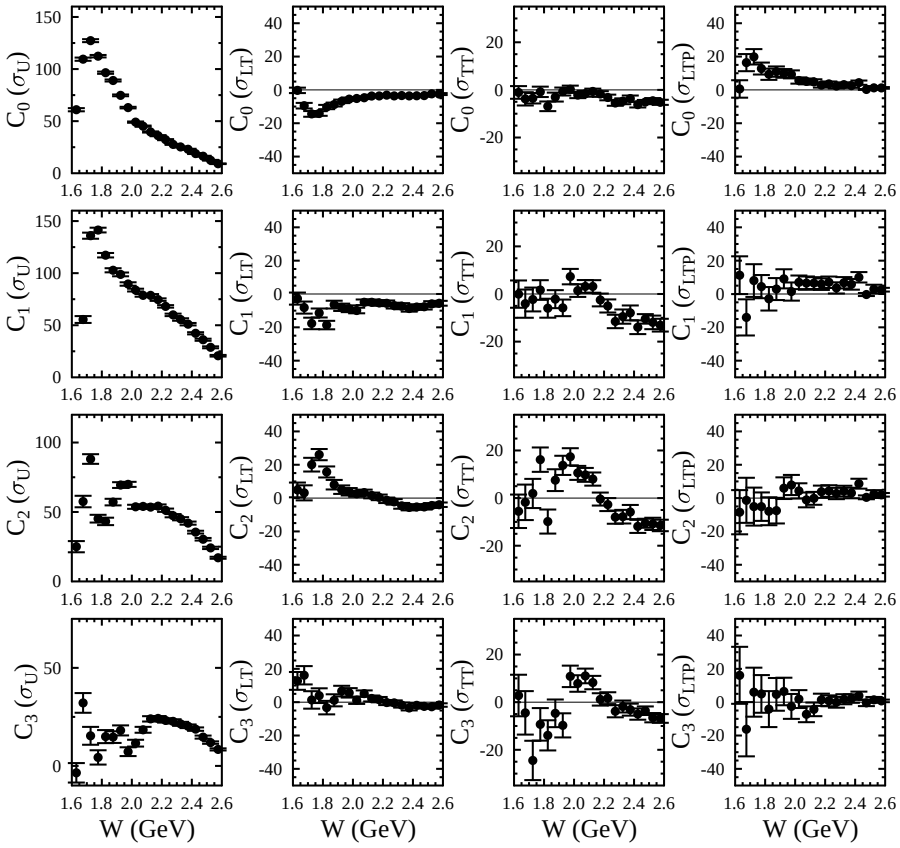

Figure 17: Legendre polynomial fit coefficients (nb) for $\ell = 0 \rightarrow 3$ vs. W for the $K^+\Lambda$ separated structure functions σ_U, σ_{LT}, σ_{TT}, and $\sigma_{LT'}$ for Q^2=1.80 GeV^2 [77].

The fits for $K^+\Lambda$ show structures for each of the three Q^2 points in the analysis (Q^2 = 1.80, 2.60, 3.45 GeV^2) at W=1.7 GeV in C_0 for both σ_U and σ_{LT}, W=1.9 GeV in C_2 and C_3 for σ_U, and W=2.2 GeV in C_3 for σ_U. The fits for $K^+\Sigma^0$ show structures at W=1.9 GeV in C_0 and C_2 for σ_U and σ_{TT}. Of course, making statements regarding the possible orbital angular momentum of the associated resonances requires care as interference effects among the different partial waves can cause strength for a given orbital angular momentum value to be spread over multiple Legendre coefficients.

In a second approach, each of the Legendre coefficients can be further expanded in terms of products of pairs of multipole amplitudes, but these expansions quickly become unwieldy as the number of participating partial waves increases. However, additional insight can be gathered from a fit to the structure functions with a coherent Legendre series of the form:

$$\frac{d\sigma_{U,LT,TT,LT'}}{d\Omega^*} = \left[\sum_{\ell=0}^{2} C_\ell(Q^2,W) P_\ell(\cos\theta_K^*)\right]^2 + C_x^2. \quad (9)$$

The coefficients $C_\ell(Q^2,W)$ are the amplitudes of the coherent S, P, and D-wave contributions, respectively, while C_x takes into account an incoherent "background" connected with higher-order terms that are not taken into account in the truncated sum. Of course, one

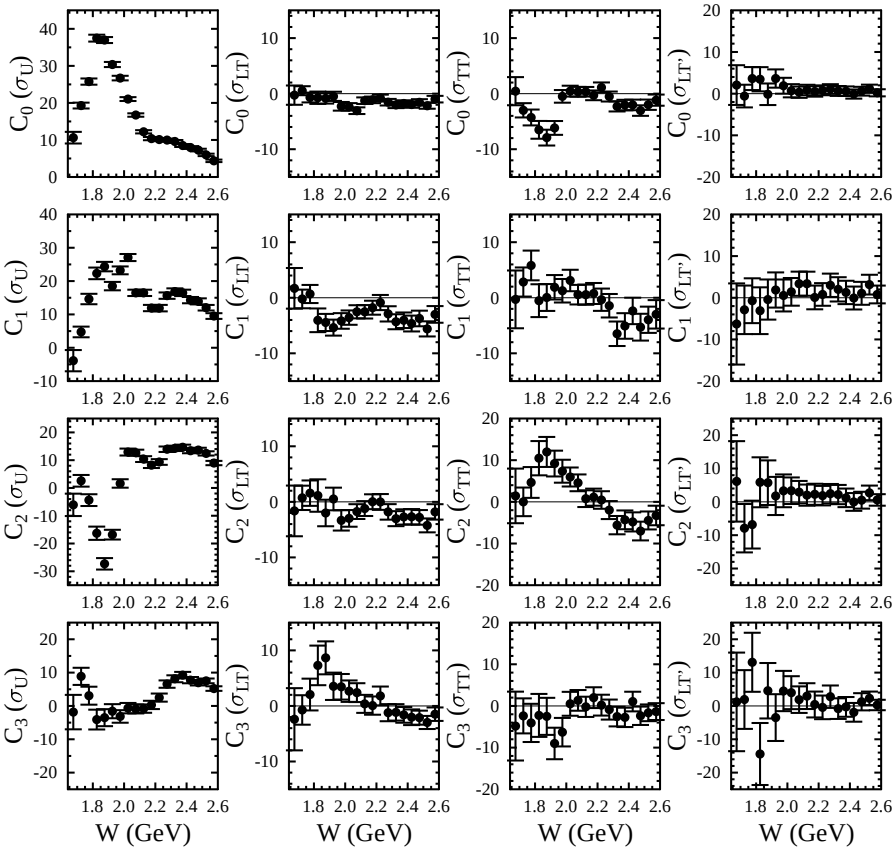

Figure 18: Legendre polynomial fit coefficients (nb) for $\ell = 0 \rightarrow 3$ vs. W for the $K^+\Sigma^0$ separated structure functions σ_U, σ_{LT}, σ_{TT}, and $\sigma_{LT'}$ for Q^2=1.80 GeV^2 [77].

must take care against making too much of the fit results using the simplistic form of Eq.(9) as it does not represent a true amplitude fit. Rather the point was to look for structures that appear at a given W and for each Q^2 for a given C_ℓ coefficient as suggestive evidence for possible N^* resonance contributions that can be studied in more detail in a more sophisticated and complete analysis. Figures 19 and 20 show the Legendre coefficients from this approach for σ_U for the $K^+\Lambda$ and $K^+\Sigma^0$ reactions, respectively, for the three Q^2 points in the analysis of Ref. [77].

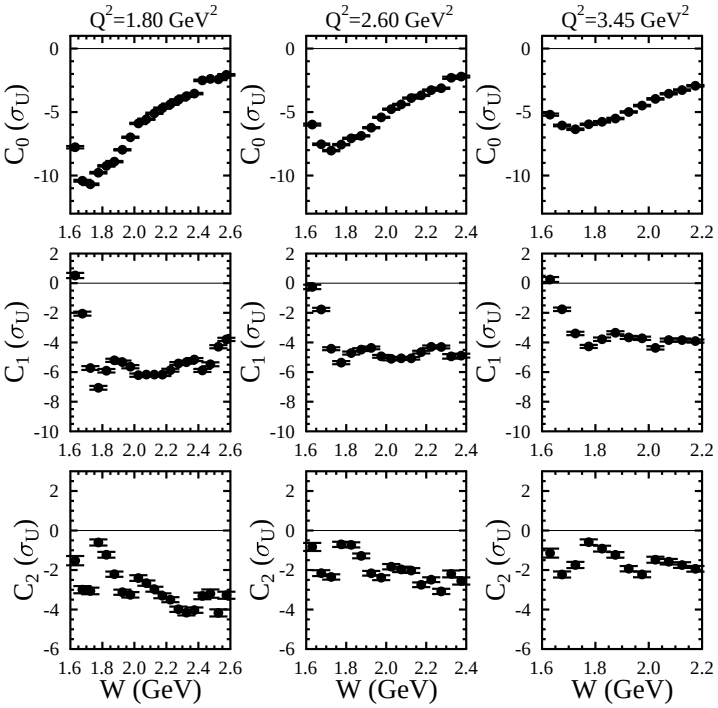

Figure 19: Coherent Legendre polynomial fit coefficients $((\mathrm{nb/sr})^{1/2})$ $\ell = 0 \rightarrow 2$ vs. W for the $K^+\Lambda$ separated structure function σ_U for Q^2=1.80, 2.60, and 3.45 GeV^2 [77].

The fit coefficients for σ_U shown in Figs. 19 and 20 show reasonable correspondence among all three Q^2 points. For the $K^+\Lambda$ fits, strength is seen at: W=1.7 GeV in C_0, W=1.9 GeV in C_1, and W=2.2 GeV in C_2. While it might be tempting to view this as corroboration of the findings of the $K^+\Lambda$ photoproduction amplitude analysis from Ref. [86], obviously more detailed work is required. For the $K^+\Sigma^0$ fits, strength is seen at W=1.85 GeV in C_0 and W=1.9 GeV in C_2. It is interesting that there is no signature of strength in the P-wave as seen through the coefficient C_1, but again a more sophisticated and complete analysis will be required to make more definitive statements. Regardless of the details and issues, these studies indicate the sensitivity of the KY final states to high-lying N^* couplings.

3.5 Development of Reaction Model

A critical aspect of this proposal is not just the measurement of the differential cross sections and separated structure functions for the $K^+\Lambda$ and $K^+\Sigma^0$ final states, but the development of a reaction model capable of describing the observables with sufficient accuracy to reliable extract the electrocoupling parameters for the dominant N^* and Δ^* states coupling to these channels. At the current time a reliable reaction model that well describes the existing CLAS

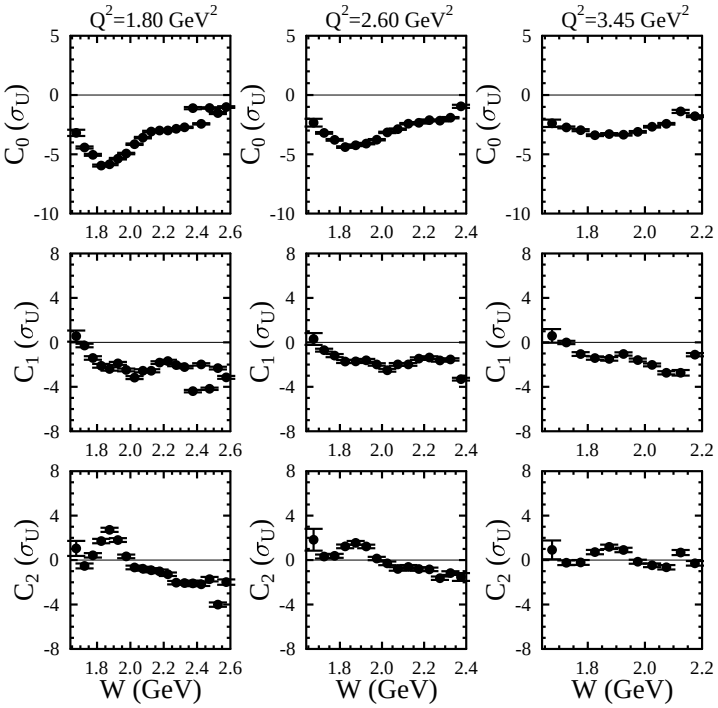

Figure 20: Coherent Legendre polynomial fit coefficients ($(\mathrm{nb/sr})^{1/2}$) $\ell = 0 \rightarrow 3$ vs. W for the $K^+\Sigma^0$ separated structure function σ_U for Q^2=1.80, 2.60, and 3.45 GeV^2 [77].

$K^+\Lambda$ and $K^+\Sigma^0$ structure functions does not yet exist. This can clearly be seen from the comparisons of the available models to the data in Figs. 13 and 14.

A key part of this new strangeness physics experiment is to extract the N^* electrocoupling parameters from the measured cross section and separated structure function data not only for the new measurements at 11 GeV beam energy, but also for the already published electroproduction data from CLAS [74, 75, 77, 79, 80, 81, 82]. In order to extract the N^* electrocoupling parameters from the data, it is essential that we have a flexible reaction model that can be tuned to precisely fit the existing CLAS KY photo- and electroproduction data and that eventually allows us to extract the N^* electrocouplings and their partial KY decay widths, fitting them to observables measured in the KY channels. One candidate is the Ghent Regge plus resonance model.

The Ghent Regge plus resonance (RPR) model [63] represents a single-channel model for KY photo- and electroproduction that is based mainly on fits to the available CLAS KY photoproduction data. This hybrid approach combines a standard effective Lagrangian isobar model to describe the s-channel N^* resonance contributions with a Reggeon-exchange formalism to describe the non-resonant t-channel background. This model has been constrained by fits to the available CLAS $\gamma p \rightarrow K^+\Lambda$ and $\gamma p \rightarrow K^+\Sigma^0$ data and thus provides a good description of the photoproduction data. As of yet, the model has not been constrained by fits to any of the available CLAS electroproduction data. However, a recent effort from the Ghent group has taken important steps to use the electroproduction data to better constrain the non-resonant amplitudes above the resonance region [87]. It is expected that this development will be able to better constrain the resonant and non-resonant contributions within the resonance region.

Based on discussions with Jan Ryckebusch as part of the developments related to this

proposal, we have laid out a series of goals that might enable us to develop the RPR model (or other suitable model) into a tool to extract the N^* electrocoupling parameters for the KY final states from both the low Q^2 CLAS data and the high Q^2 CLAS12 data in a phased approach. The key steps in this phased approach include:

Goal #1: To detail the complete list of N^* states included in the most recent version of the model along with their electrocoupling parameters for both the $K^+\Lambda$ and $K^+\Sigma^0$ final states.

Goal #2: In order to provide consistency with the electrocoupling parameters determined from fits to the CLAS $N\pi$ and $N\pi\pi$ data sets, update the model with the N^* parameters from these analyses. Depending on how different these new parameters are from what is already included in the model, new data fits may have to be performed to re-establish the model resonant/non-resonant parameters.

Goal #3: In order to develop a true extraction model from the available reaction model, refit the model to the CLAS photo- and electroproduction data (Q^2 up to 4 GeV^2) with the existing non-resonant parameters constrained to their measured uncertainties and extract the electrocoupling parameters and KY decay widths for all prominent N^* states that couple to the $K^+\Lambda$ and $K^+\Sigma^0$ exclusive channels. Given the significant amount of data involved, this work will require studies of the stability of the fit results and the sensitivities to the different data sets given their quoted systematic uncertainties.

This work will eventually lead to a fourth goal to further develop the model to be able to include the new KY data for W up to 3 GeV and Q^2 up to 10 - 12 GeV^2 that can be used as input for coupled-channel model development in these kinematics. Work to develop this reaction model are now getting underway and the plan is to have it sufficiently developed on a time-scale appropriate for the new measurements from this proposal.

4 Experiment Details

We plan to measure the exclusive $K^+\Lambda$ and $K^+\Sigma^0$ final states using the CLAS12 spectrometer in Hall B at Jefferson Laboratory using a longitudinally polarized electron beam. At an incident beam energy of 11 GeV, we will measure the differential cross sections over a range of invariant energy $1.6 < W < 3$ GeV in the virtually unexplored domain of momentum transfers Q^2 from 4 to 12 GeV^2, while spanning the full center-of-mass angular range of the final state K^+. Note that while the goal is to explore couplings of N^* and Δ^* states in the mass range from 1.6 to 3 GeV, we will perform our analysis over the range of invariant energy W up to 4 GeV due to the large hadronic decays widths for these high-lying states. Measurements in the range of $Q^2 < 4$ GeV^2 will also be completed in order to provide sufficient overlap to connect to the existing CLAS KY data from Ref. [77].

Fits to the Φ dependence of the differential cross sections for the $K^+\Lambda$ and $K^+\Sigma^0$ final states will be carried out to determine the separated structure functions $\sigma_U \equiv \sigma_T + \epsilon\sigma_L$, σ_{TT}, and σ_{LT}. Fits to the beam spin asymmetry will be carried out to determine the polarized structure function $\sigma_{LT'}$. The separated structure functions will be extracted as a function of Q^2, W, and $\cos\theta^*_K$, using the well-established techniques that were developed from analysis of these same final states from the CLAS program [74, 77]. Note that a separation of σ_L and σ_T is not required for this proposal as the longitudinal amplitudes can be probed with greater sensitivity from the interference structure functions σ_{LT} and $\sigma_{LT'}$.

In the second stage of the analysis, the N^* and Δ^* electrocoupling parameters will be extracted from fits to the separated structure function data using either an existing reaction model such as the Regge plus resonance model from Ghent [63] (see Section 3.5) or a phenomenological approach that is analogous to those developed in recent years for analysis of the CLAS $N\pi$ and $N\pi\pi$ data sets. These include the UIM isobar model [33] and an approach based on dispersion relations for the $N\pi$ channel [29] and the $N\pi\pi$ channels [32, 42]. The extraction of the electrocoupling amplitudes will be completed separately for both the $K^+\Lambda$ and $K^+\Sigma^0$ channels, but the fits will be carried out with a common set of electrocoupling parameters. These results can be compared with the $\gamma_v NN^*$ electrocouplings available from the studies of the $N\pi\pi$ channel. These fits will provide a set of initial N^* electrocoupling amplitudes. A final evaluation of N^* electrocoupling amplitudes will be carried out within the framework of the most advanced coupled channel approaches, which are currently being developed by the Argonne-Osaka Collaboration [5] and the GWU group [88]. Both of these approaches account for the contributions of all relevant meson-baryon open channels and their hadronic interactions. Ultimately, they will include updates from JPARC measurements on the $\pi N \to \pi\pi N$ reaction at W values covered by this proposal [89]. Consistent results on the $\gamma_v NN^*$ electrocouplings from independent analyses of the $N\pi$, $N\pi\pi$ and KY channels and extracted from the global coupled channel analysis will provide the final reliable extraction of these fundamental quantities.

4.1 CLAS12 Simulations

This experiment will employ the base CLAS12 detector subsystems. In order to study the detector response and to model the CLAS12 acceptance function, the standard CLAS12 fast Monte Carlo (fastMC) suite was employed. This simulation code included the nominal detector geometries and the expected position and time resolutions for the detectors for

the reconstruction of the four-momenta of the final state particles. The event generator was based on a PYTHIA phase space model modified to reflect the expected Q^2 dependence of the incident virtual photon flux and the t-dependence of the final state K^+ seen from Ref. [77]. Figure 21 shows the kinematics of the generated events at a beam energy E_b=11 GeV as a function of Q^2, W, and $\cos\theta^*_K$. The corresponding distributions of these quantities from our CLAS data set at E_b=5.5 GeV are shown in Fig. 22 for comparison. The p vs. θ laboratory distributions for the final state charged particles e', K^+, p, and π^- are shown in Fig. 23. These figures show that the e', K^+, and p are mostly directed toward the CLAS12 forward detector system ($\theta < 35°$), while the π^- tracks mostly are contained within the CLAS12 central detector system ($\theta > 35°$).

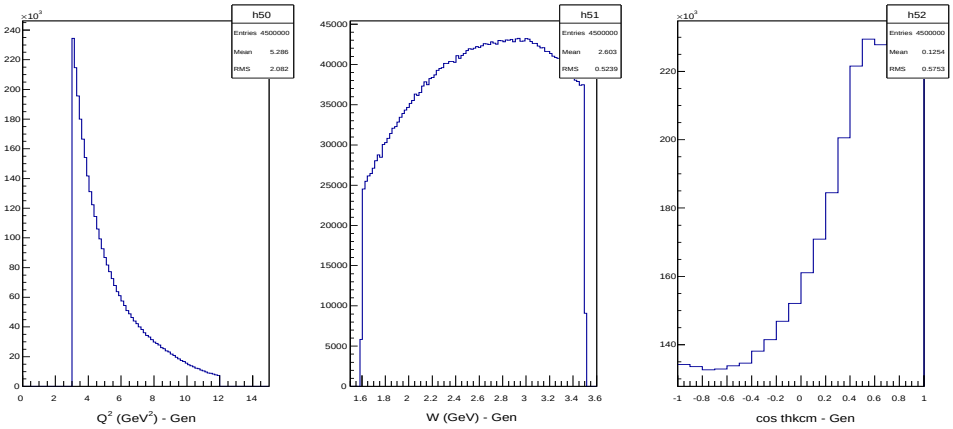

Figure 21: Distributions of Q^2, W, and $\cos\theta^*_K$ for the generated modified phase space Monte Carlo K^+Y events used to determine the CLAS12 acceptance functions for this proposal. Note that the sharp edges seen in the Q^2 and W distributions here are due to the kinematic bounds selected for the event generation.

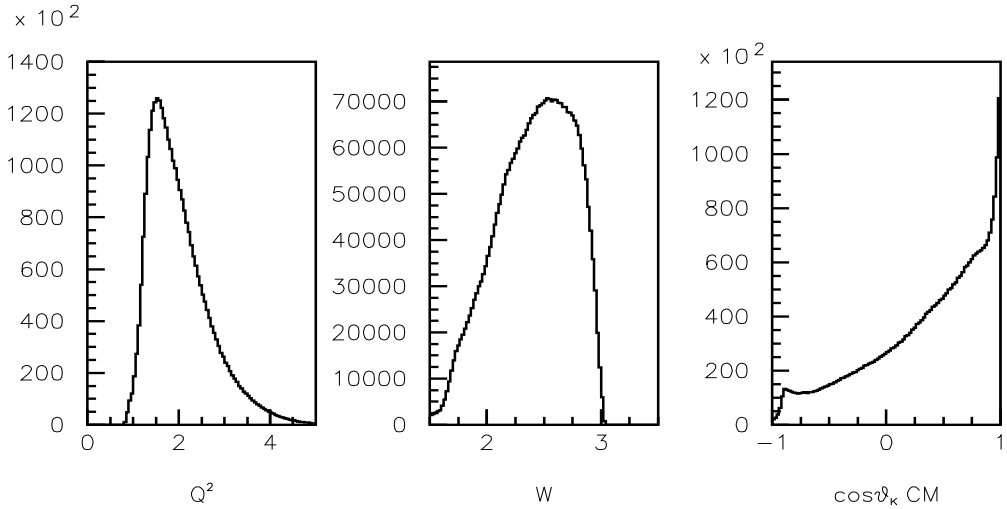

Figure 22: Distributions of Q^2, W, and $\cos\theta^*_K$ for the CLAS e1f data set at E_b=5.5 GeV for K^+Y events.

The momentum distribution for the final state K^+ is important to consider given the particle identification capabilities of CLAS12. The reconstructed K^+ momenta will be in the range from 0.5 to 7 GeV. Figure 24 shows the correlation of the K^+ momenta as a

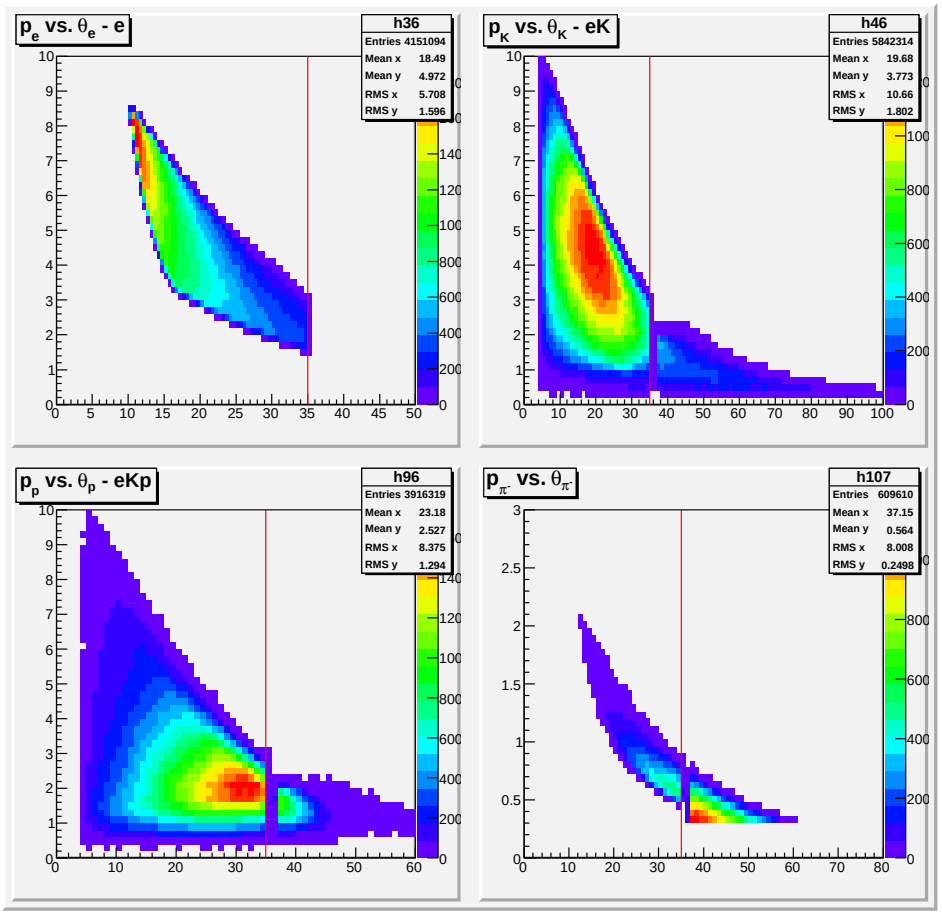

Figure 23: Distributions of laboratory momentum (GeV) vs. polar angle (deg) for the final state e' (UL), K^+ (UR), p (LL), and π^- (LR) for the reaction $ep \rightarrow e'K^+\Lambda$. The discontinuity at $\theta = 35°$ (noted by the vertical red lines) is due to the acceptance gap between the CLAS12 forward and central detectors.

function of Q^2 from our Monte Carlo data over the kinematic range of this proposal. The average K^+ momentum is about 4 GeV, with a relatively weak dependence on Q^2 for the kinematic extent of this study.

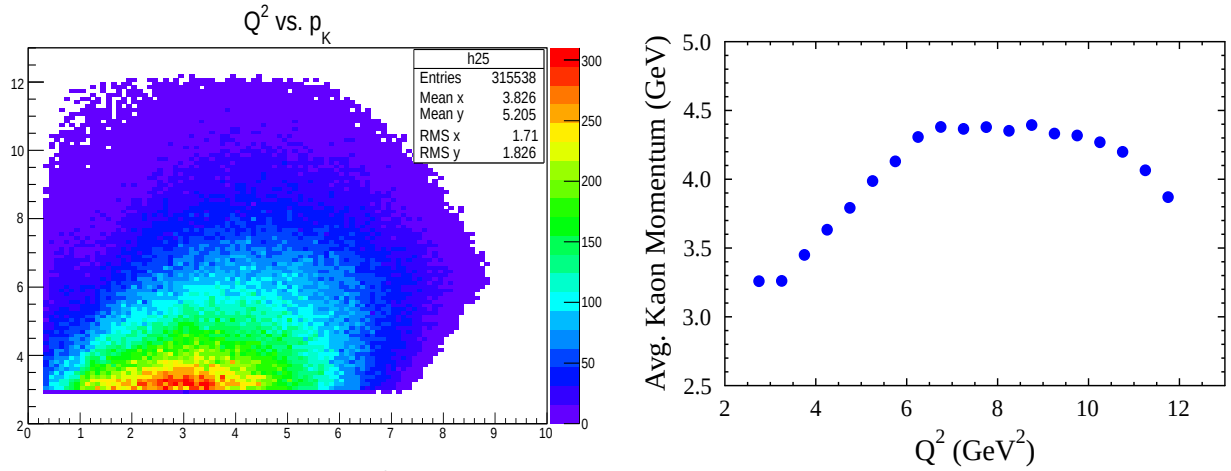

Figure 24: Distribution of Q^2 vs. K^+ momentum (left) and the average K^+ momentum vs. Q^2 (right) for the generated modified phase space Monte Carlo $K^+\Lambda$ events.

Figure 25 shows the particle identification capabilities expected for the CLAS12 Forward Time-of-Flight (FTOF) system based on the flight time differences between charged hadrons as a function of momentum. The primary issue with the final state reconstruction will be separating K^+ tracks from the dominant π^+ background. The FTOF system was designed to separate K^+ tracks from π^+ tracks up to ~3 GeV with 4σ separation (assuming an average FTOF resolution of 80 ps). However, 1σ separation based on the nominal system design up to 6 GeV is provided. However, these statements are believed to be *extremely* conservative. Based on the measured resolutions for the new FTOF panel-1b counters, 2σ separation of π/K tracks up to 6 GeV should be achievable. Final state K^+ identification will thus rely mostly on the FTOF particle identification capabilities over the full K^+ momentum range.

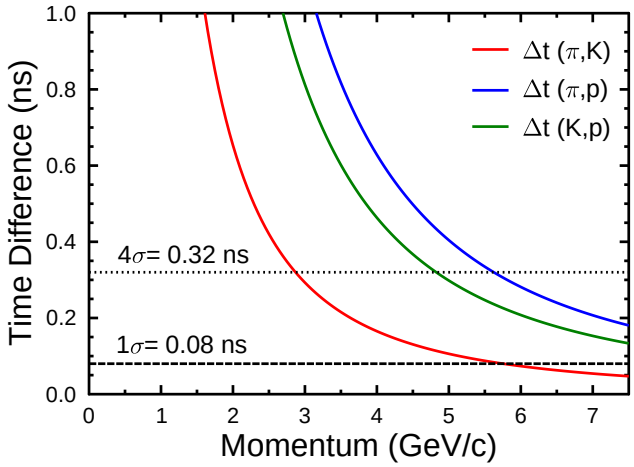

Figure 25: Difference in charged hadron flight times from the event vertex to the FTOF system as a function of hadron momentum showing the differences between π/K (red curve), π/p (blue curve), and K/p (green curve). The 4σ and 1σ FTOF time resolution lines are shown.

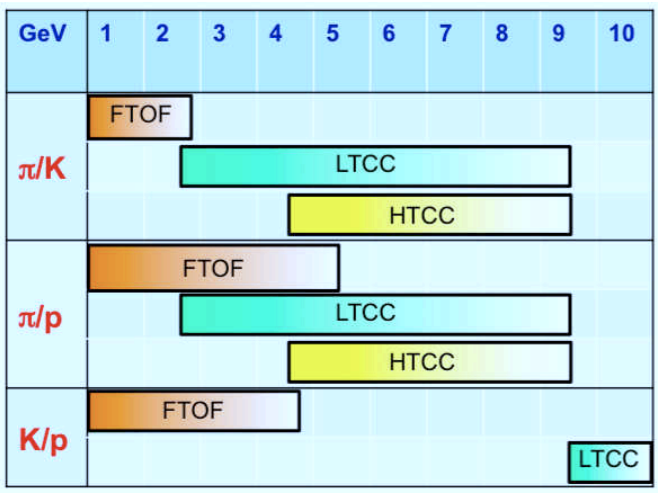

Figure 26: Representation of which CLAS12 subsystems are employed for charged hadron identification as a function of momentum.

Particle identification in CLAS12 is actually accomplished through the use of multiple detection subsystems, including not only the FTOF, but also the two Cherenkov detector systems, the Low Threshold Cherenkov Counter (LTCC) and the High Threshold Cherenkov Counter (HTCC). Figure 26 shows a representation of which subsystems are employed for charged hadron identification as a function of momentum. The LTCC in its nominal active area is expected to be 95 - 99% efficient for π/K separation in the range of momenta from 3.0 to 9.5 GeV. The HTCC is expected to be 95-99% efficiency for π tracks from 5.0 to 9.5 GeV. Efficiency factors of 95% within the associated momentum ranges given here are assumed in the Monte Carlo for the LTCC and HTCC detectors within the particle identification routine.

Note also that detection of the final state proton from the Λ hyperon mesonic decay (B.R.=63.9%) will allow us to further reduce the underlying backgrounds employing a cut on the $MM^2(e'K^+p)$ distribution to select events with a missing π^- or a missing $\pi^-\gamma$ (see Fig. 27). This will allow for fits that separate the $K^+\Lambda$, $K^+\Sigma^0$, and background contributions with different systematics. Comparison of cross sections extracted using the $e'K^+$ final state topology to that from the $e'K^+p$ final state topology will be used to assess the systematic uncertainties associated with the background subtraction and fitting algorithms used to separate the $K^+\Lambda$ and $K^+\Sigma^0$ event samples from the $e'K^+$ missing mass distributions for each bin of Q^2, W, $\cos\theta^*_K$, and Φ. A discussion of systematic uncertainty evaluation for the CLAS e1f K^+Y analysis related to the data in Ref. [77] is included in Ref. [90].

Representative hyperon missing mass spectra for both the detected $e'K^+$ and $e'K^+p$ final state topologies are shown in Fig. 28. For these studies, three different reactions were simulated, including the hyperon channels of interest, $K^+\Lambda$ and $K^+\Sigma^0$, as well as the predominant background channel $ep \rightarrow e'p\pi^+\pi^-$, where the final state π^+ is misidentified as a K^+. These studies employed $N_{K\Lambda}/N_{K\Sigma}$=3 based on the ratios seen in the CLAS e1c and e1f data sets (which span $0.5 < Q^2 < 3.9$ GeV^2, W up to 2.6 GeV). The background channel was assumed to have three times the integrated yield as the $K^+\Lambda$ channel in the mass range shown, again based on the findings from the CLAS e1c and e1f data sets. For the $e'K^+p$ topology, a cut has been placed on the $MM^2(e'K^+p)$ distribution in the range from 0 to

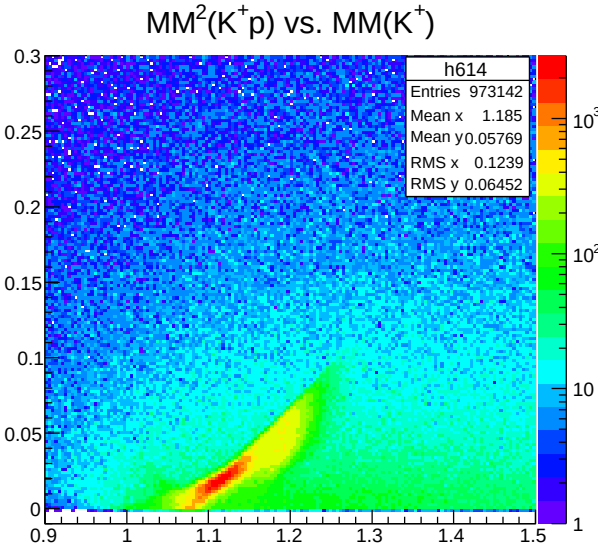

Figure 27: Correlation of the reconstructed $MM^2(e'K^+p)$ (GeV^2) vs. $MM(e'K^+)$ (GeV) distributions from the Monte Carlo studies.

0.065 GeV^2 to reduce the background (see Fig. 27).

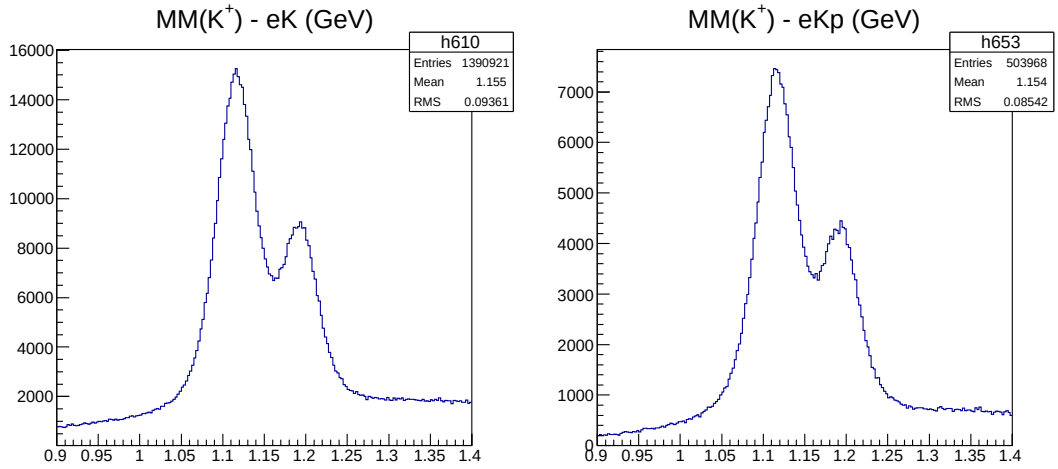

Figure 28: Missing mass spectra $MM(e'K^+)$ (left) for the reconstructed $e'K^+$ final state topology and (right) for the $e'K^+p$ final state topology from the Monte Carlo studies showing the separation of the $K^+\Lambda$ and $K^+\Sigma^0$ final state events.

Figure 29 shows the expected missing mass resolution of CLAS12 as a function of Q^2 and W summed over all other kinematic variables. The average missing mass resolution is roughly σ_{MM}=22 MeV. This is only about 50% worse than the CLAS spectrometer resolution for the 6 GeV electroproduction data sets. The resolution is relatively flat with W. However, the resolution function has a strong dependence on Q^2, ranging from 20 MeV at low Q^2 to nearly 40 MeV at high Q^2. Further work will be needed to develop approaches for fitting the missing mass spectra to separate the $K^+\Lambda$, $K^+\Sigma^0$, and background channels. However, the algorithms successfully employed for the analysis of Ref. [77] (see Ref. [90]) will be used as a starting point. Note as well that the simulation results shown include only final-state

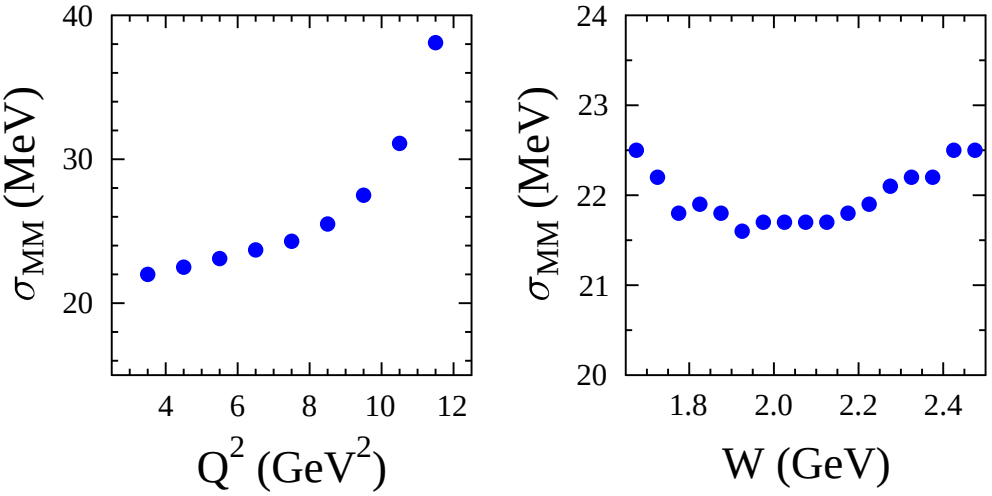

Figure 29: Hyperon missing mass $MM(e'K^+)$ resolution from reconstructed $ep \to e'K^+\Lambda$ and $ep \to e'K^+\Sigma^0$ Monte Carlo data as a function of (left) Q^2 (averaged over W and $\cos\theta^*_K$) and (right) W (averaged over Q^2 and $\cos\theta^*_K$).

radiative effects, and thus do not represent a full treatment. However, the degree of overlap between the Λ and Σ^0 peaks is expected to be reasonably accurate as reflected in Fig. 28.

4.2 Count Rate Estimates - $K^+\Lambda$ and $K^+\Sigma^0$ Channels

The K^+Y differential cross section in a given bin of Q^2, W, $\cos\theta^*_K$, and Φ can be written as:

$$\frac{d\sigma}{d\Omega^*_K} = \frac{1}{\mathcal{L}} \cdot \frac{N}{ACC \cdot (\Delta Q^2 \Delta W \Delta \cos\theta^*_K \Delta\Phi)} \cdot \frac{1}{\Gamma_v} \cdot \frac{1}{t}, \tag{10}$$

where $\mathcal{L}$ is the beam-target luminosity, N is the number of counts in the bin, ACC is the CLAS12 acceptance for the bin (including all inefficiencies, branching ratios, and dead times), Γ_v is the virtual photon flux factor, and t is the run duration.

Bin	Q^2 (GeV^2)	W (GeV)
1	4.5	1.725
2	4.5	1.925
3	6.5	1.725
4	6.5	1.925
5	8.5	1.725
6	8.5	1.925
7	10.5	1.725
8	10.5	1.925

Table 3: The eight representative bins in Q^2 and W used for the count rate estimates in this proposal.

To determine the expected yields for this experiment, estimates for the $K^+\Lambda$ and $K^+\Sigma^0$ final states were carried out for the eight representative Q^2/W bins shown in Table 3. These

include two values of W (1.725, 1.925 GeV) and four values of Q^2 (4.5, 6.5, 8.5, 10.5 GeV^2). In addition, the following assumptions were made:

- $\mathcal{L} = 1 \times 10^{35}$ cm^{-2}s^{-1} - nominal CLAS12 design operating luminosity
- Full torus field with negatively charged particles inbending
- $t = 60$ days (compatible with run group that includes E12-09-003)
- Γ_v from Eq.(3)
- $d\sigma/d\Omega$ from a $1/Q^2$ extrapolation of the form:

$$d\sigma/d\Omega = \mathcal{C}_1 \cdot \left(\mathcal{C}_2 + Q^2\right)^{-1} \tag{11}$$

  to the electroproduction cross sections in each $\cos\theta^*_K$ bin shown in Figs. 15 and 16.

- Binning:
  - $\Delta Q^2 = 1.0$ GeV^2
  - $\Delta W = 50$ MeV,
  - $\Delta \cos\theta^*_K$ 10 bins:
    [-0.90,-0.65], [-0.65,-0.40], [-0.40,-0.20], [-0.20,0.00], [0.00,0.20], [0.20,0.40], [0.40,0.60], [0.60,0.75], [0.75,0.90], [0.90,1.00]
  - $\Delta\Phi$: 8 bins 45°-wide [-180°,180°]
    ($\cos\theta^*_K$ and Φ binning chosen to match e1f analysis)
- *ACC* from fastMC with a reasonably realistic event distribution for the event generator as shown in Fig. 21.

The acceptances in each kinematic bin were determined from the ratio of reconstructed to generated events in each bin. The acceptances determined for the $K^+\Lambda$ final state for the $e'K^+$ and $e'K^+p$ topologies are shown in Fig. 30 for the eight bins of Table 3 averaged over Φ. The acceptances for the $K^+\Sigma^0$ final state are comparable. The studies show typical Φ-averaged $e'K^+$ topology acceptances of 55% and typical Φ-averaged $e'K^+p$ topology acceptances of 25%, relatively independent of kinematics.

Figure 31 shows the expected yields determined using Eq.(10) for the $K^+\Lambda$ final state for both the $e'K^+$ and $e'K^+p$ topologies and Fig. 32 shows the expected yields for the $K^+\Sigma^0$ final state. Also shown in these figures are the counts from the e1f analysis at Q^2=1.8 GeV^2 (from Ref. [77]) for the $e'K^+$ topology, which we might consider as a reasonable measure of the required statistics for a viable experiment. From the favorable comparison between the expected yields for this experiment compared to the yields from the CLAS e1f data set, this experiment at 11 GeV with CLAS12 is considered as quite feasible. Note the $1/Q^2$ extrapolation was found to be the most reasonable to fit the existing CLAS data in the range of Q^2 up to 4 GeV^2. However, the expected yields were also studied using a $1/Q^4$ extrapolation of the cross sections in Figs. 15 and 16 as:

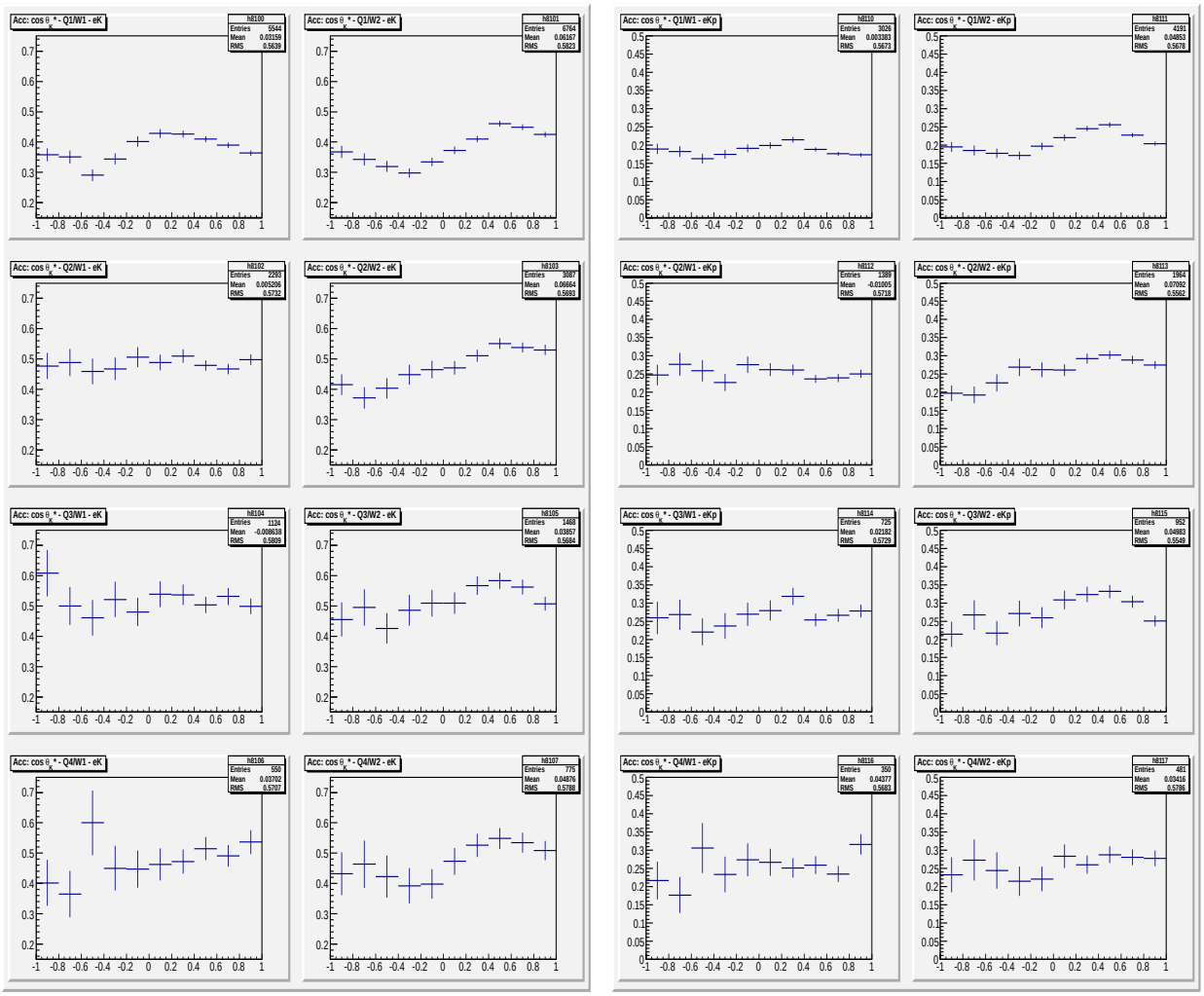

Figure 30: Acceptance functions determined from the Monte Carlo simulations as a function of $\cos\theta_K^*$ averaged over Φ for the $K^+\Lambda$ final state for the $e'K^+$ topology (left) and the $e'K^+p$ topology (right) for the eight Q^2/W bins listed in Table 3. These acceptances were determined with a thrown event sample of 10M events and yield statistical uncertainties on the acceptance of a few percent.

$$d\sigma/d\Omega = \mathcal{C}_1 \cdot \left(\mathcal{C}_2 + Q^2\right)^{-2}, \tag{12}$$

and the corresponding expected yields were reduced by a factor of two. There is a definite uncertainty with these sorts of extrapolations. The best fits for the low Q^2 CLAS data are not necessarily expected to reflect the reality of our high Q^2 data due to the different associated dynamics. In this regard, the Moscow State University group is currently exploring the possibility of extrapolating the available CLAS KY data employing the fully integrated cross section extrapolated as:

$$\sum_{\tau} C_\tau \left(\frac{M^2}{Q^2}\right)^{\frac{\tau-2}{2}}, \quad \tau = 2,\ 4,\ 6, \ldots, \tag{13}$$

with parameters C_τ and M fit independently to the available CLAS data in each bin of W. Such an approach has provided predictions for the Q^2 evolution of the CLAS $N\pi\pi$ electroproduction cross sections for $5 < Q^2 < 12$ GeV^2 as published in Ref. [91].

4.2.1 Alternative Topologies

As with all studies of hyperon electroproduction, the success of the experiment is directly correlated with the size of the final statistical uncertainties, assuming that the systematic uncertainties associated with the subtraction of the dominant π^+ misidentification background and the Λ/Σ^0 separation can be controlled over the kinematic domain studied. In an effort to maximize the hyperon yield relative to the background, several additional event topologies have been studied in detail beyond those for $e'K^+$ and $e'K^+p$.

If we attempt to reduce the backgrounds associated with π^+ misidentification, we could consider an experiment reconstructing solely the p and π^- from the Λ mesonic decay in addition to the scattered electron. However, due to the fact that most π^- tracks go into the CLAS12 central detector with $p < 300$ MeV (see Fig. 23), and this represents the effective momentum threshold for tracks to traverse the central trackers and the Central Time-of-Flight (CTOF) system, this topology only has a typical acceptance of $\sim$3% (including the $\Lambda \rightarrow p\pi^-$ B.R.=63.9%). This final state topology is therefore certainly not viable for a precision experiment.

In an attempt to improve the separation of Λ and Σ^0 hyperons in the $MM(e'K^+)$ spectrum, we could consider detecting the γ from the $\Sigma^0 \rightarrow \Lambda\gamma$ decay (B.R.=100%) in the CLAS12 PCAL. However, the γ momentum distribution has a typical value of $\sim$150 MeV. For such energies the PCAL photon detection efficiency is only $\sim$50% with a very steep gradient (see Fig. 33). Thus any topology requiring photon detection for Σ^0 reconstruction is deemed as not viable.

4.3 Count Rate Estimates - Phase 2 Channels

The main emphasis of this proposal is a detailed study of the associated production of the ground state hyperons through the reactions:

$$e + p \rightarrow e' + K^+ + \Lambda \tag{14}$$

$$e + p \rightarrow e' + K^+ + \Sigma^0. \tag{15}$$

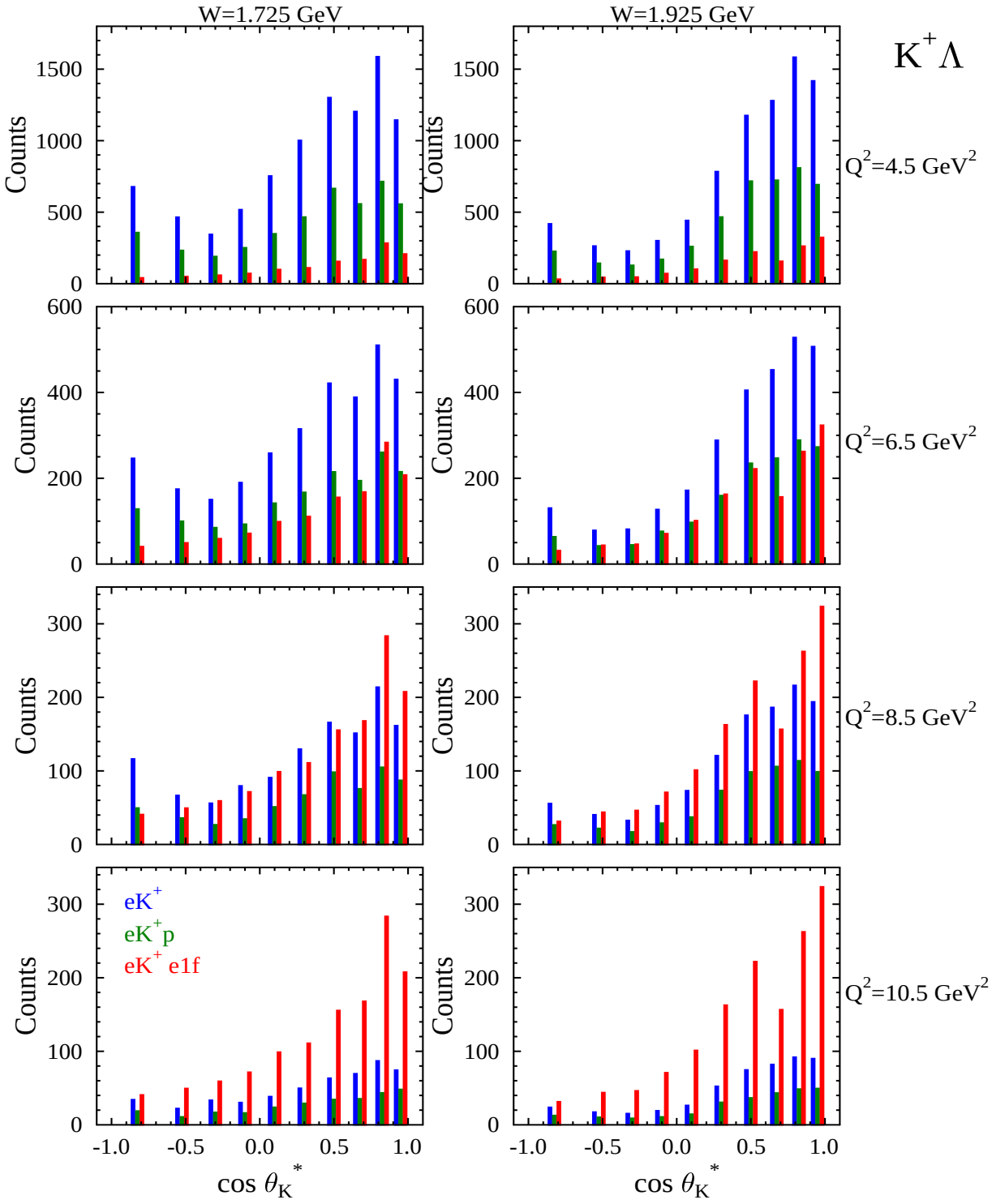

Figure 31: Expected counts in the eight bins of Table 3 at Q^2=4.5, 6.5, 8.5, and 10.5 GeV^2 for the $K^+\Lambda$ final state at two representative values of W=1.725, 1.925 GeV averaged over Φ for a 60 day run at a luminosity of 1×10^{35} cm^{-2}s^{-1} for the $e'K^+$ topology (green bars) and $e'K^+p$ topology (blue bars) compared to the $e'K^+$ yields from the e1f experiment at Q^2=1.8 GeV^2 (red bars) of Ref. [77].

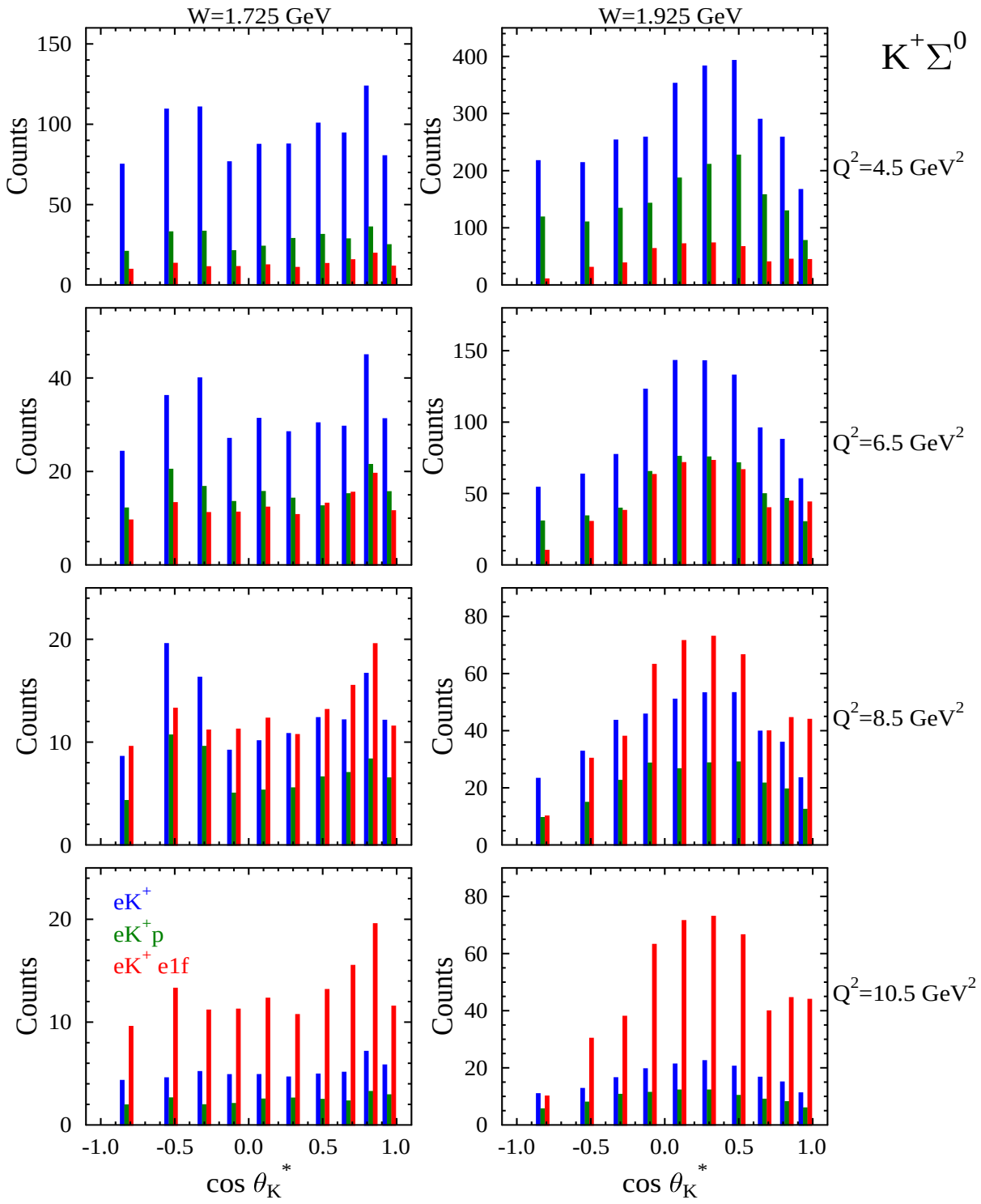

Figure 32: Expected counts in the eight bins of Table 3 at Q^2=4.5, 6.5, 8.5, and 10.5 GeV^2 for the $K^+\Sigma^0$ final state at two representative values of W=1.725, 1.925 GeV averaged over Φ for a 60 day run at a luminosity of 1×10^{35} cm^{-2}s^{-1} for the $e'K^+$ topology (green bars) and $e'K^+p$ topology (blue bars) compared to the $e'K^+$ yields from the e1f experiment at Q^2=1.8 GeV^2 (red bars) of Ref. [77].

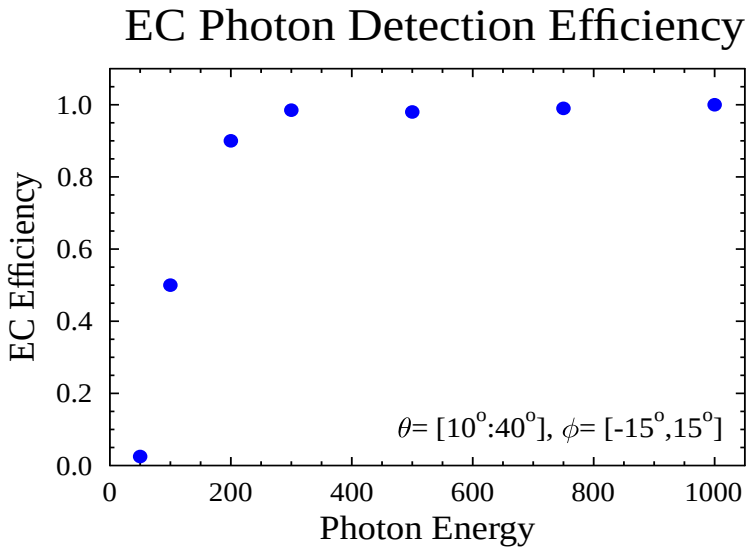

Figure 33: Simulation results of the photon detection efficiency for the CLAS EC detectors as a function of photon energy. The photon detection efficiency for the CLAS12 PCAL is expected to be quite similar.

These "phase 1" reaction channels were chosen because they have the largest cross sections and the highest acceptances of the various strangeness channels.

As stated in Section 1, the second phase of this proposal includes studies of the strangeness channels with smaller cross sections and detector acceptances. Among the considered reactions include:

$$e + p \rightarrow e' + K^{*+} + \Lambda \tag{16}$$
$$e + p \rightarrow e' + K^{*+} + \Sigma^0 \tag{17}$$
$$e + p \rightarrow e' + K^{+} + \Lambda(1405) \tag{18}$$
$$e + p \rightarrow e' + K^{+} + \Lambda(1520) \tag{19}$$
$$e + p \rightarrow e' + K^{+} + \Sigma^0(1385) \tag{20}$$
$$e + p \rightarrow e' + K^{0}_{s} + \Sigma^{+} \tag{21}$$
$$e + p \rightarrow e' + K^{*0} + \Sigma^{+}. \tag{22}$$

The yield estimates for each of these "phase 2" reactions were made relative to the yield for the $K^+\Lambda$ reaction. As no electroproduction cross sections are yet available, the photoproduction cross sections were extrapolated using the form of Eq.(11). The acceptance function of CLAS12 for the different final states used the same fastMC code suite already discussed with a phase space model governing the energy and angular distribution of the final state particles.

In the following subsections, relevant details on each of the phase 2 reactions is provided. Table 4 contains the count rate expectations relative to the phase 1 channels. Given the lower yields for analysis, it will certainly be the case that larger bin sizes in Q^2, W, and $\cos\theta^*_K$ will be required relative to those selected for the K^+Y channels. Unless the expected cross sections are substantially larger from the estimates considered here, the measurements

will in all likelihood be limited to differential cross sections only. However, attempts to perform Φ fits to extract the structure functions can possibly be made in some cases, such as bins at low Q^2 and forward kaon CM angles.

Group	Reaction	$\langle d\sigma/d\Omega\rangle$ (nb/sr)	$\langle ACC\rangle$	Yield Ratio
	$e+p \to e' + K^+ + \Lambda$	200	55%	1.000
	$e+p \to e' + K^+ + \Sigma^0$	50	55%	0.250
A	$e+p \to e' + K^{*+} + \Lambda$	10	6%	0.005
	$e+p \to e' + K^{*+} + \Sigma^0$	10	6%	0.005
B	$e+p \to e' + K^+ + \Lambda(1405)$	10	11%	0.010
	$e+p \to e' + K^+ + \Lambda(1520)$	20	10%	0.019
	$e+p \to e' + K^+ + \Sigma^0(1385)$	40	5%	0.017
C	$e+p \to e' + K^0_s + \Sigma^+$	10	6%	0.006
	$e+p \to e' + K^{*0} + \Sigma^+$	10	6%	0.006

Table 4: Count rate estimates for the various phase 2 strangeness reaction channels considered. The "yield ratio" column shows the yields expected relative to the $K^+\Lambda$ channel. The cross section column is the expected cross section for the different channels at Q^2=1.8 GeV^2. The average acceptance column takes into account the branching ratios for the reconstructed final state(s) considered.

4.3.1 Group A - $ep \to e'K^{*+}Y$

Present coupled channel analyses have been focused mainly on fits to data of πN, ηN, and KY production. However, studies of the K^*Y channels (see Eq.(16) and Eq.(17)) are also expected to provide unique and relevant information regarding production of high-lying N^* states. The quark model calculations of Ref. [92] showed that several N^* states are predicted to couple to the KY and K^*Y channels with similar strength. These include the $D_{13}(2080)$, $S_{11}(2090)$, and $G_{17}(2190)$. Comparisons of the K^+Y and $K^{*+}Y$ cross sections for these states will be relevant to study the different production mechanisms involved.

The reconstruction of the $K^{*+}\Lambda$ and $K^{*+}\Sigma^0$ final states will proceed through identification of the final state K^{*+} with the hyperon identified using the missing-mass technique. The K^{*+} will be identified from the decay:

$$\begin{aligned} K^{*+} \to \quad & K^0_s\ \pi^+ \qquad (B.R. = 50\%) \\ & \hookrightarrow K^0_s \to \pi^+\pi^- \quad (B.R. = 69.2\%). \end{aligned} \tag{23}$$

The reconstructed reaction is: $ep \to e'\pi^+\pi^-\pi^+(\Lambda)$ or $ep \to e'\pi^+\pi^-\pi^+(\Sigma^0)$.

The cross section estimates for these channels are based on extrapolations from the CLAS photoproduction data from Ref. [93]. The typical cross sections averaged over W and $\cos\theta^*_{K^*}$ at the photon point are 16 nb/sr. The average CLAS12 acceptance for this reaction, accounting for the relevant branching fractions, is estimated to be ∼6%.

4.3.2 Group B - $ep \rightarrow e'K^+Y^*$

The $\Lambda(1405)$ is situated just below the $N\bar{K}$ threshold and has been an enigmatic state in the spectrum of strange baryons for many years. Only recently have precision photoproduction data from CLAS become available that have started to shed some light on the production dynamics [94, 95]. The $\Lambda(1405)$ sits between the $\Sigma(1385)$ and the $\Lambda(1520)$ hyperons. Simultaneous studies of all three states should be expected to yield insight into their production dynamics, which should lead to further insight into their structures. To date the available theoretical models that have studied $N^* \rightarrow KY^*$ decays have produced mixed results on whether s-channel resonance contributions play any significant role [96, 97, 98, 99].

The reconstruction of the three K^+Y^* channels (see Eq.(18), Eq.(19), and Eq.(20)) was considered as follows:

$$ep \rightarrow e'K^+\,\Lambda(1405) \tag{24}$$
$$\hookrightarrow\ \Lambda(1405) \rightarrow \pi^-\Sigma^+ \qquad (B.R. = 18\%) \tag{25}$$
$$\hookrightarrow\ \Lambda(1405) \rightarrow \pi^+\Sigma^- \qquad (B.R. = 18\%) \tag{26}$$

The reconstructed reactions are: $ep \rightarrow e'K^+\pi^-(\Sigma^+)$ and $ep \rightarrow e'K^+\pi^+(\Sigma^-)$.

$$ep \rightarrow e'K^+\,\Lambda(1520) \tag{27}$$
$$\hookrightarrow\ \Lambda(1520) \rightarrow K^-p \qquad (B.R. = 50\%) \tag{28}$$

The reconstructed reactions are: $ep \rightarrow e'K^+K^-(p)$ and $ep \rightarrow e'K^+p(K^-)$.

$$ep \rightarrow e'K^+\,\Sigma^0(1385) \tag{29}$$
$$\hookrightarrow\ \Sigma^0(1385) \rightarrow \Lambda\pi^0 \qquad (B.R. = 87\%) \tag{30}$$
$$\hookrightarrow \Lambda \rightarrow p\pi^- \qquad (B.R. = 64\%) \tag{31}$$

The reconstructed reaction is: $ep \rightarrow e'K^+p\pi^-(\pi^0)$.

As no electroproduction cross sections are yet available for these final states, extrapolations of the available CLAS photoproduction cross sections of Ref. [95] were employed. The typical cross sections averaged over W and $\cos\theta^*_K$ at the photon point are 16 nb/sr for $K^+\Lambda(1405)$, 32 nb/sr for $K^+\Lambda(1520)$, and 65 nb/sr for $K^+\Sigma^0(1385)$. The average CLAS12 acceptances for these reactions, accounting for the relevant branching fractions are estimated to be 11% for $K^+\Lambda(1405)$, 10% for $K^+\Lambda(1520)$, and 5% for $K^+\Sigma^0(1385)$.

4.3.3 Group C - $ep \rightarrow e'K^{(*)0}\Sigma^+$

Study of the strangeness production of different isospin partners in the final state, namely Σ^+ production vs. Σ^0 production (see Eq.(22)), is also a necessary part of developing complete reaction models. For example, the dynamics of K^{*0} production are simplified relative to K^{*+} production as K^{*0} exchange in the t-channel is strongly suppressed [100]. Thus studies of both the charged and neutral mesons in the final state may allow for scrutiny of the

developed reaction models that can give additional insight into the different isospin channels and their coupling to the final state N^*s.

The reconstruction of these $K^{(*)0}\Sigma^+$ channels was considered as follows:

$$ep \rightarrow e'\, K^0_s\, \Sigma^+ \tag{32}$$

$$\hookrightarrow K^0_s \rightarrow \pi^+\pi^- \qquad (B.R. = 69\%) \tag{33}$$

The reconstructed reaction is: $ep \rightarrow e'\pi^+\pi^-(\Sigma^+)$.

$$ep \rightarrow e'\, K^{*0}\, \Sigma^+ \tag{34}$$

$$\hookrightarrow\ K^{*0} \rightarrow K^+\pi^- \qquad (B.R. = 67\%) \tag{35}$$

The reconstructed reaction is: $ep \rightarrow e'K^+\pi^-(\Sigma^+)$.

The cross section for the $K^0_s\Sigma^+$ reaction was based on available CLAS photoproduction data from Ref. [93]. The typical value averaged over W and $\cos\theta^*_K$ is 16 nb/sr. For the $K^{*0}\Sigma^+$ channel, the average cross section from CLAS photoproduction data of Ref. [101] over W and $\cos\theta^*_K$ is estimated to be 16 nb/sr. The average CLAS12 acceptances for these reactions was found to be 6%.

5 Summary and Beam Time Request

The studies of the electromagnetic transition amplitudes between the nucleon ground and excited states over a wide range of Q^2, elucidate the relevant degrees of freedom in the N^* structure at different distance scales and will allow for a better understanding of the non-perturbative strong interaction that governs the formation of the N^* states. With the JLab 12-GeV upgrade and the new CLAS12 detector, a unique opportunity is available to probe the structure of nucleon resonances at high Q^2. These studies will address some of the most fundamental issues of present-day hadron physics [4]:

1. What is the mechanism of confinement?
2. How is confinement related to the mass generating mechanism of dynamical chiral symmetry breaking?
3. Can the fundamental QCD Lagrangian successfully describe the complex structure of the states of different quantum numbers in the N^* spectrum?

These questions are very difficult to answer, but there is great promise of a much improved understanding through the experiments that will take place with CLAS12. Studies of the behavior of the N^* resonances at high Q^2 provide a decisive advantage, as the meson cloud contributions become small and the quark core contributions that we seek to study dominate the dynamical response.

In recent years the CLAS Collaboration has succeeded in determining the Q^2 evolution of baryon resonance electrocoupling amplitudes from unpolarized $N\pi$ and $N\pi\pi$ electroproduction data. Consistent results for both channels have been extracted through two conceptually different approaches (isobar model and dispersion relations). These results unambiguously show that the resonance parameters can be extracted with unprecedented accuracy for excited states in the region $W < 1.7$ GeV and $Q^2 < 4.5$ GeV^2 for single non-strange meson final states and in the region $W < 2.0$ GeV and $Q^2 < 1.5$ GeV^2 for double charged pion final states. These studies make clear that the independent analysis of multiple final states in the same kinematic domain is essential to minimize the systematics of the measurements and to have confidence in the extracted electrocoupling parameters. In terms of pionic coupling, most high-lying N^* states preferentially decay through the $N\pi\pi$ channel instead of the $N\pi$ channel. Thus data from the KY channels is critical to provide an independent extraction of the electrocoupling amplitudes for the high-lying N^* states against those determined from the analysis of the $N\pi\pi$ channel.

In conjunction with the already approved CLAS12 experiment E12-09-003 [11] that will study N^* states that couple to the single non-strange meson and $N\pi\pi$ channels, this experiment will focus on the study of N^* states that couple to the KY strangeness final states. Together the proponents of these two experiments seek to extract the electrocouplings of all prominent N^* and Δ^* excited states spanning the full nucleon resonance region, up to W=3 GeV in the almost unexplored region of Q^2 from 4 to 12 GeV^2. As part of these efforts, work is underway to develop advanced reaction models to reliably extract the $\gamma_v NN^*$ electrocouplings over the range of photon virtualities up to Q^2=12 GeV^2. These models will explicitly take into account the contributions from quark-gluon degrees of freedom. The models developed to fit the single non-strange meson and $N\pi\pi$ data sets will be extended

in scope to incorporate the KY exclusive channels.

The results obtained for the $N\pi$ and $N\pi\pi$ data already represent consistent initial estimates of the Q^2 evolution of the low-lying N^* electrocoupling parameters. This information will be checked and extended in a global and complete coupled-channels analysis of all major meson electroproduction channels including the KY data that incorporate the amplitudes of non-resonant electroproduction mechanisms extracted from the CLAS and CLAS12 data using the phenomenological approaches developed to study the data.

In addition, studies of the Q^2 evolution of the electrocoupling amplitudes for the high-lying N^* states that couple to the KY final states, make it possible to study the data for evidence regarding hybrid baryons in which massive confined gluons play a role equal to that of valence quarks. The high Q^2 regime makes access to the quark-gluon structure of hybrid states less obscured by effects of the meson-baryon dressing. These studies are also vital to confirm or reject the signals claimed for new candidate baryon states recently observed in analyses of KY photoproduction [58].

These experiments to study N^* and Δ^* electroproduction at high Q^2 represent an extension of the existing program from the low Q^2 CLAS analyses into a domain that will allow direct access to quarks decoupled from the meson-baryon cloud. Experiment E12-09-003 has been approved as part of a CLAS12 run group with 60 days of beam time. This new experiment to study N^* decays to the KY final states is envisioned to be part of this run group as well, acquiring data under the same conditions. These include a highly polarized 11 GeV electron beam on an unpolarized liquid-hydrogen target, with the CLAS12 readout defined by the standard electron trigger requirement and with the torus field polarity set for inbending of negatively charged particles. The first phase of the analysis will be to perform measurements for the highest yield strangeness channels associated with the $K^+\Lambda$ and $K^+\Sigma^0$ final states. The second phase of the analysis will focus on lower yield channels such as $K^0\Sigma^+$, K^*Y, and KY^*.

All of these efforts will be greatly enhanced by the new CLAS12 detector, which will provide simultaneous data for a wide range of N^* states from all of the major exclusive meson electroproduction channels, which theorists can use to untangle the competing contributions that enter each state in a different way. A coordinated effort between experimental and theoretical physicists is required.

This proposal requests no new beam time. It has been designed to be fully compatible to fit within the CLAS12 run group already approved for 60 days of beam time using a highly polarized electron beam at 11 GeV incident upon an unpolarized liquid-hydrogen target at a beam-target luminosity of $\mathcal{L} = 1 \times 10^{35}$ cm^{-2}s^{-1}. The CLAS12 detector need only be configured with its nominal base equipment. We request that the JLab PAC approve this experiment and recognize its importance as a critical and necessary extension to the CLAS12 N^* program at high Q^2. This proposal has been reviewed internally within the CLAS Collaboration and has been fully endorsed as a CLAS Collaboration proposal.

6 Participation of Research Groups

University of South Carolina

Ralf Gothe from the University of South Carolina is not only a spokesperson of this proposal, but also is a spokesperson of the related CLAS12 N^* experiment E12-09-003. He will be involved in not only data analysis issues pertaining to this data set, but also on working to develop the associated reaction models and the fitting algorithms for the higher-level analysis that will ultimately be required for extraction of the electrocoupling parameters of the N^* resonance states. Ralf Gothe's group was also responsible for the assembly and calibration of the high resolution FTOF panel-1b counters that represent the main subsystem to be employed for charged particle identification in this experiment.

Center for Nuclear Studies - GW Data Analysis Center

The George Washington University Data Analysis Center is actively involved in an extensive research program on the theoretical interpretation of the results from the proposed experiment. In particular, the GW group will provide an extended analysis of the πN, NN, KY, γN, and $\gamma^* N$ processes on the time scale of the completion of this experiment.

Lattice Group at the JLab Theory Center

Members of the Lattice Group at the JLab Theory Center are actively involved in an extensive research program on the theoretical interpretation of the results from the proposed experiment. In particular, the group will provide LQCD calculations of transition helicity amplitudes and/or related form factors for several excited proton states of various quantum numbers at photon virtualities of the proposed experiment on the time scale the completion of this experiment.

JLab Physics Analysis Center

The JLab Physics Analysis Center that was formed after the culmination of the Excited Baryon Analysis Center (EBAC) is actively involved in an extensive research program on the theoretical interpretation of the results from the proposed experiment. In particular, this group will help to develop analysis methods for interpreting the extracted N^* form factors in Q^2 to 12 GeV^2 in terms of DSE and LQCD predictions on the time scale of the completion of this experiment.

Argonne-Osaka Group

Members of the Argonne-Osaka Group are actively engaged in extending the analysis of meson production amplitudes through their dynamical coupled-channel approach that was started under the aegis of the JLab Excited Baryon Analysis Center (EBAC). This group is working to extract the mass, coupling constants, and electromagnetic transition form factors of the N^* states across the full resonance region at photon virtualities relevant for this experiment on a time scale compatible with the completion of this experiment.

Argonne National Lab

The Argonne National Lab (ANL) contributors to this proposal are actively involved in an extensive research program on the theoretical interpretation of the results from the proposed experiment. In particular, ANL group will provide calculations of transition helicity amplitudes and/or related form factors for several excited proton states of various quantum numbers within the framework Dyson-Schwinger on the time scale of the completion of this experiment.

Ghent University

Members of the Ghent group are actively involved in the development of reaction models for KY electroproduction that are being employed as the basis for the development of a complete model that will be used to describe the KY energy and angular of distributions this experiment and of the existing KY electroproduction data from CLAS at lower Q^2. This model is necessary to extract the electrocoupling parameters for the dominant N^* and Δ^* states coupling to the strangeness channels.

Old Dominion University

Kijun Park from Old Dominion University was a lead author on the CLAS analysis of the separated structure functions and induced polarization for the KY final states. He has also lead the analysis of the separated structure functions for the $N\pi$ CLAS data with the subsequent extraction of the electrocoupling parameters for resonances in the region of W=1.6 GeV. He will be involved in multiple aspects of the analysis of the data to extract cross sections and the higher-level analysis to extract the helicity amplitudes.

Florida International University

Brian Raue from Florida International University is a lead author on the majority of the CLAS KY electroproduction papers from the analysis of the separated structure functions, to the extraction of the single and double polarization observables. He will be involved in multiple aspects of the data analysis for this experiment.

Moscow State University

The Moscow State University group will participate in the development of the simulation (GEANT4) and reconstruction software, trigger, and data acquisition. MSU will develop and support the special database needed for N^* studies in the coupled-channel analysis.

University of Iowa

Haiyun Lu from the University of Iowa has been involved as a lead author on analysis of CLAS KY^* photoproduction data. He will be involved in multiple aspects of the data analysis for this experiment.

Ohio University

Ken Hicks from Ohio University has been involved in the CLAS strangeness physics program as a lead author on the analysis of data for the $K^{*+}Y$ and $K^{*0}Y$ channels in

photoproduction. He has also played an important role in related analysis and publications as a collaborator at LEPS. He will be involved in multiple aspects of the data analysis for this experiment with a focus on some of the more promising phase 2 reactions.

References

[1] N. Isgur and G. Karl, Phys. Rev. D **19**, 2653 (1979); S. Capstick and N. Isgur, Phys. Rev. D **34**, 2809 (1986).

[2] M. Aiello, M.M. Giannini, and E. Santopinto, J. Phys. G **24**, 753 (1998); M. De Sanctis *et al.*, Phys. Rev. C **76**, 062202 (2007).

[3] I.G. Aznauryan, Phys. Rev. C **76**, 025212 (2007).

[4] I.G. Aznauryan *et al.*, Int. J. Mod. Phys. **E22**, 1330015 (2013).

[5] H. Kamano, S.X. Nakamura, T.-S.H. Lee, and T. Sato, Phys. Rev. C **88**, 035201 (2013).

[6] I. Aznauryan *et al.*, arXiv:0907.1901, (2009).

[7] I.G. Aznauryan *et al. (CLAS Collaboration)*, Phys. Rev. C **80**, 055203 (2009).

[8] V.I. Mokeev and I.G. Aznauryan, Int. J. Mod. Phys. Conf. Ser. **26**, 1460080 (2014).

[9] S. Capstick and B. Keister, Phys. Rev. D **51**, 3598 (1995).

[10] B. Julia-Diaz *et al.*, Phys. Rev. C **77**, 045205 (2008).

[11] R.W. Gothe *et al.*, JLab Experiment E12-09-003.

[12] U. Löhring, B.C. Metsch, and H.R. Petry, Eur. Phys. J. A **10**, 395 (2001).

[13] J. Beringer *et al.* (PDG), Phys. Rev. D **86**, 010001 (2012).

[14] B. Julia-Diaz, D.O. Riska, and F. Coester, Phys. Rev. C **79**, 035212 (2004).

[15] C.S. An *et al.*, Phys. Rev. C **74** 055205 (2006).

[16] M. Bhagwat and P. Tandy, AIP Conf. Proc. **842**, 225 (2006).

[17] C.D. Roberts, Prog. Part. Nucl. Phys. **61**, 55 (2008).

[18] C. Chen *et al.*, Few Body Syst. **53**, 293 (2012).

[19] V. Pascalutsa, M. Vanderhaeghen, and S.N. Yang, Phys. Rept. **437**, 125 (2007).

[20] M.V. Polyakov and K.M. Semenov-Tian-Shansky, Eur. Phys. J. A **40**, 181 (2009).

[21] USQCD Collaboration, http://www.usqcd.org/collaboration.html.

[22] P.O. Bowman *et al.*, Phys. Rev. D **71**, 054507 (2005).

[23] I.C. Cloët, C.D. Roberts, and A.W. Thomas, Phys. Rev. Lett **111**, 101803 (2013).

[24] L.L. Frankfurt *et al.*, Phys. Rev. Lett. **84**, 2589 (2000).

[25] K. Goeke, M.V. Polyakov, and M. Vanderhaeghen, Prog. Part. Nucl. Phys. **47**, 401 (2001).

[26] White Paper of the JLab Workshop, *"Electromagnetic N-N* Transition Form Factors"*, Newport News, VA, USA, October 13-15, 2008.

[27] V.D. Burkert and T.S.-H. Lee, Int. J. Mod. Phys. **E13**, 1035 (2004).

[28] V.D. Burkert, Prog. Part. Nucl. Phys. **55**, 108 (2005).

[29] I. Aznauryan, Phys. Rev. C **67**, 015209 (2003).

[30] I.G. Aznauryan *et al.*, Phys. Rev. C **72**, 045201 (2005).

[31] I.G. Aznauryan *et al. (CLAS Collaboration)*, Phys. Rev. C **78**, 045209 (2008).

[32] V. Mokeev *et al. (CLAS Collaboration)*, Phys. Rev. C **86**, 035203 (2012).

[33] L. Tiator *et al.*, Eur. Phys. J. ST **198**, 141 (2011).

[34] R.A. Arndt, J.M. Ford, and L.D. Roper, Phys. Rev. D **32**, 1085 (1985).

[35] R. Arndt *et al.*, Phys. Rev. C **74**, 045205 (2006).

[36] M. Dugger *et al. (CLAS Collaboration)*, Phys. Rev. C **79**, 065206 (2009).

[37] V.D. Burkert *et al.*, Phys. Rev. C **67**, 035204 (2003).

[38] C.E. Carlson and N.C. Mukhopadhyay, Phys. Rev. Lett. **67**, 3745 (1991).

[39] Z. Li, Phys. Rev. D **44**, 2841 (1991).

[40] T. Barnes, nucl-th/0009011. Proceedings of COSY Workshop on Baryon Excitations, May (2000).

[41] V.D. Burkert and I. Aznauryan, AIP Conf. Proc. **1182**, 900 (2009).

[42] V.I. Mokeev *et al.*, Phys. Rev. C **80**, 045212 (2009).

[43] Z.P. Li, V.D. Burkert, and Zh. Li, Phys. Rev. D **46**, 70 (1992).

[44] T. Barnes and F.E. Close, Phys. Lett. B **123**, 89 (1983).

[45] L. Kisslinger *et al.*, Phys. Rev. D **51**, R5986 (1995).

[46] N. Isgur and J.E. Paton, Phys. Lett. **124 B**, 247 (1983); Phys. Rev. D **31**, 2910 (1985).

[47] J.J. Dudek and R.G. Edwards, Phys. Rev. C **85**, 054016 (2012).

[48] M. Anselimo *et al.*, Rev. Mod. Phys. **65**, 1199 (1993).

[49] M. Kirchbach *et al.*, Phys. Rev. D **64**, 114005 (2001).

[50] R.L. Jaffe and F. Wilczek, Phys. Rev. Lett. **91**, 232003 (2003).

[51] R.L. Jaffe, Phys. Rept. **409**, 1 (2005).

[52] E. Santopinto, Phys. Rev. C **72**, 022201 (2005).

[53] A.V. Sarantsev *et al.*, Eur. Phys. J. A **25**, 441 (2005).

[54] V. Shklyar, H. Lenske, and U. Mosel, Phys. Rev. C **72**, 015210 (2005).

[55] T. Mart, AIP Conf. Proc. **1056**, 31 (2008).

[56] V.A. Nikonov *et al.*, Phys. Lett. B **662**, 245 (2008).

[57] R.K. Bradford *et al. (CLAS Collaboration)*, Phys. Rev. C **75**, 035205 (2007).

[58] A.V. Anisovich *et al.*, Eur. Phys. J A **48**, 15 (2012).

[59] E. Klempt and R. Workman, https://pdg.web.cern.ch/pdg/2012/reviews/rpp2012-rev-n-delta-resonances.pdf.

[60] B. Julia-Diaz *et al.*, Nucl. Phys. A **755**, 463 (2005); B. Julia-Diaz *et al.*, Phys. Rev. C **73**, 055204 (2006).

[61] T. Mart and A. Sulaksono, Phys.Rev. C **74**, 055203 (2006).

[62] A.V. Anisovich *et al.*, Eur. Phys. J. A **48**, 88 (2012).

[63] T. Corthals *et al.*, Phys. Lett. B **656**, 186 (2007).

[64] O. Maxwell, Phys. Rev. C **85**, 034611 (2012).

[65] R. Bradford *et al. (CLAS Collaboration)*, Phys. Rev. C **73**, 035202 (2006).

[66] M.E. McCracken *et al. (CLAS Collaboration)*, Phys. Rev. C **81**, 025201 (2010).

[67] B. Dey *et al. (CLAS Collaboration)*, Phys. Rev. C **82**, 025202 (2010).

[68] C.W. Akerlof *et al.*, Phys. Rev. **163**, 1482 (1967).

[69] Some authors use a pre-factor for the σ_L (σ_{LT}) term of ϵ_L ($\sqrt{2\epsilon_L(\epsilon+1)}$) instead, where $\epsilon_L = \epsilon Q^2/\nu_{cm}^2$ parameterizes the longitudinal polarization of the virtual photon. Some also take a $\sin\theta_K^*$ ($\sin^2\theta_K^*$) term out of the definition of σ_{LT} (σ_{TT}).

[70] T. Mart, Int. J. Mod. Phys. E **19**, 2343 (2010).

[71] O. Maxwell, Phys. Rev. C **76**, 014621 (2007).

[72] O. Maxwell, Phys. Rev. C **86**, 064612 (2012).

[73] S. Janssen *et al.*, Phys. Rev. C **67**, 052201 (R) (2003).

[74] P. Ambrozewicz *et al. (CLAS Collaboration)*, Phys. Rev. C **75**, 045203 (2007).

[75] R. Nasseripour *et al. (CLAS Collaboration)*, Phys. Rev. C **77**, 065208 (2008).

[76] T. Mart, Eur. Phys. J. Web Conf. **3**, 07002 (2010).

[77] D.S. Carman *et al. (CLAS Collaboration)*, Phys. Rev. C **87**, 025204 (2013).

[78] T. Mart, Phys. Rev. C **82**, 025209 (2010).

[79] D.S. Carman *et al. (CLAS Collaboration)*, Phys. Rev. Lett. **90**, 131804 (2003).

[80] D.S. Carman *et al. (CLAS Collaboration)*, Phys. Rev. C **79**, 065205 (2009).

[81] M. Gabrielyan *et al. (CLAS Collaboration)*, AIP Conf.Proc. **1432**, 375 (2012); M. Gabrielyan *et al. (CLAS Collaboration)*, to be submitted to Phys. Rev. C, (2014).

[82] B.A. Raue and D.S. Carman, Phys. Rev. C **71**, 065209 (2005).

[83] A. de la Puente, O. Maxwell, and B.A. Raue, Phys. Rev. C **80**, 065205 (2009).

[84] M. Guidal, J.M. Laget, and M. Vanderhaegen, Nucl. Phys. A **627**, 645 (1997); Phys. Rev. C **61**, 025204 (2000); Phys. Rev. C **68**, 058201 (2003).

[85] W. Bartel *et al.*, Nucl. Phys. B **58**, 429 (1973).

[86] R.A. Schumacher and M.M. Sargsian, Phys. Rev. C **83**, 025207 (2011).

[87] T. Vrancx, J. Ryckebusch, and J. Nys, arXiv:1404.4156, (2014).

[88] M. Döring, Int. J. Mod. Phys. Conf. Ser. **26**, 1460054 (2014).

[89] JPARC Experiment P45, *3-Body Hadronic Reactions for New Aspects of Baryon Spectroscopy*, K.H. Hicks and H. Sako spokesperson.

[90] http://clasweb.jlab.org/rungroups/e1f/carman/e1f-note-v3.pdf

[91] V. Burkert *et al.*, Bull. Moscow State University, Ser. Phys. **2**, 49 (2014).

[92] S. Capstick and W. Roberts, Phys. Rev. D **58**, 074011 (1998).

[93] W. Tang *et al. (CLAS Collaboration)*, Phys. Rev. C **87**, 065204 (2013).

[94] K. Moriya *et al. (CLAS Collaboration)*, Phys. Rev. C **87**, 035206 (2013).

[95] K. Moriya *et al. (CLAS Collaboration)*, Phys. Rev. C **88**, 045201 (2013).

[96] Y.Oh, C.M. Ko, and K. Nakayama, Phys. Rev. C **77**, 045204 (2008).

[97] S.-I. Nam, A. Hosaka, and H.-C. Kim, Phys. Rev. D **71**, 114012 (2005).

[98] J. He and X.-R. Chen, Phys. Rev. C **86**, 035204 (2012).

[99] S.-I. Nam, J.-H. Park, A. Hosaka, and H.-C. Kim, J. Korean Phys. Soc. **59**, 2676 (2011).

[100] Q. Zhao, J.S. Al Khalili, and C. Bennhold, Phys. Rev. C **64**, 052201 (R) (2001).

[101] I. Hleiqawi *et al. (CLAS Collaboration)*, Phys. Rev. C **75**, 042201 (R) (2007).